HHS Public Access

Author manuscript

Cell Rep. Author manuscript; available in PMC 2021 May 19.

Published in final edited form as:

Cell Rep. 2021 April 13; 35(2): 108980. doi:10.1016/j.celrep.2021.108980.

Huntingtin-mediated axonal transport requires arginine methylation by PRMT6

Alice Migazzi[1,2,3,17], **Chiara Scaramuzzino**[7,17], **Eric N. Anderson**[8], **Debasmita Tripathy**[1], **Ivó H. Hernández**[9,10], **Rogan A. Grant**[8], **Michela Roccuzzo**[11], **Laura Tosatto**[12], **Amandine Virlogeux**[7], **Chiara Zuccato**[13,14], **Andrea Caricasole**[15], **Tamara Ratovitski**[16], **Christopher A. Ross**[16], **Udai B. Pandey**[8], **José J. Lucas**[9,10], **Frédéric Saudou**[7,*], **Maria Pennuto**[2,3,4,5,6,*], **Manuela Basso**[1,18,*]

[1]Laboratory of Transcriptional Neurobiology, Department of Cellular, Computational and Integrative Biology – CIBIO, University of Trento, Trento 38123, Italy

[2]Dulbecco Telethon Institute, Department of Cellular, Computational and Integrative Biology – CIBIO, University of Trento, Trento 38123, Italy

[3]Department of Biomedical Sciences (DBS), University of Padova, Padova 35131, Italy

[4]Veneto Institute of Molecular Medicine (VIMM), via Orus 2, Padova 35129, Italy

[5]Padova Neuroscience Center (PNC), Padova 35131, Italy

[6]Myology Center (CIR-Myo), Padova 35131, Italy

[7]Univ. Grenoble Alpes, Inserm, U1216, CHU Grenoble Alpes, Grenoble Institut Neurosciences, GIN, Grenoble 38000, France

[8]Department of Pediatrics, Children's Hospital of Pittsburgh, University of Pittsburgh Medical Center, Pittsburgh, PA 15224, USA

[9]Centro de Biología Molecular "Severo Ochoa" (CBMSO) CSIC/UAM, Madrid, Spain

[*]Correspondence: frederic.saudou@inserm.fr (F.S.), maria.pennuto@unipd.it (M.P.), manuela.basso@unitn.it (M.B.).

AUTHOR CONTRIBUTIONS

A.M. designed and performed the HTT, arginine methylation, and PRMT6 immunoprecipitation experiments; performed immunoblotting, immunofluorescence, neuronal, and cellular viability assays; performed the PLA in neurons, the HTT trafficking experiments, and the neuronal and striatal cell fractionation experiments; performed the *in vitro* methylation assays with GST-HTT fusion proteins and histone H3; cloned all the vectors used in this work; and analyzed the data, assembled the figures, and assisted with the writing of the paper. C.S. designed, performed, and analyzed the experiments of HTT and BDNF trafficking in microchambers; performed and analyzed electron microscopy experiments; conducted immunofluorescence of cortical and striatal neurons; and designed the fractionation experiments for both brain and neuronal fractions. D.T. performed the PLA in STHdh cells. I.H.H. performed the immunoblotting of PRMT6 in human samples. L.T. supervised the expression and purification of recombinant GST-HTT for the *in vitro* methylation assay. A.V. prepared the samples for the MS of HTT in vesicles. C. Z. provided reagents and experimental advice all throughout the work. T.R. performed the MS of HTT and arginine methylation and discussed the results. A.C., C.A.R., and J.J.L. discussed the results of the paper. U.B.P. performed the experiments in flies and discussed the paper. F.S. designed and provided experimental advice for the experiments on trafficking, helped with the writing of the paper, and contributed with laboratory support. M.P. designed and provided experimental advice for the molecular biology part regarding the arginine methylation of HTT, helped with the writing of the paper, and contributed with laboratory support and management. M.B. designed the study experiments, led the study and the collaborations, and took overall responsibility for the writing of the manuscript with contribution from all authors.

SUPPLEMENTAL INFORMATION

Supplemental information can be found online at https://doi.org/10.1016/j.celrep.2021.108980.

DECLARATION OF INTERESTS

The authors declare no competing interests.

[10]Networking Research Center on Neurodegenerative Diseases (CIBERNED), Instituto de Salud Carlos III, Madrid 28029, Spain

[11]Advanced Imaging Core Facility, Department of Cellular, Computational and Integrative Biology – CIBIO, University of Trento, Trento 8123, Italy

[12]Institute of Biophysics, National Research Council (CNR) Trento unit, Trento 38123, Italy

[13]Department of Biosciences, University of Milan, Milan, Italy

[14]Istituto Nazionale di Genetica Molecolare “Romeo ed Enrica Invernizzi,” Milan 20122, Italy

[15]Department of Neuroscience, IRBM S.p.A., Rome 00071, Italy

[16]Division of Neurobiology, Department of Psychiatry and Behavioral Sciences, Johns Hopkins University School of Medicine, Baltimore, MD 21205, USA

[17]These authors contributed equally

[18]Lead contact

SUMMARY

The huntingtin (HTT) protein transports various organelles, including vesicles containing neurotrophic factors, from embryonic development throughout life. To better understand how HTT mediates axonal transport and why this function is disrupted in Huntington’s disease (HD), we study vesicle-associated HTT and find that it is dimethylated at a highly conserved arginine residue (R118) by the protein arginine methyltransferase 6 (PRMT6). Without R118 methylation, HTT associates less with vesicles, anterograde trafficking is diminished, and neuronal death ensues—very similar to what occurs in HD. Inhibiting PRMT6 in HD cells and neurons exacerbates mutant HTT (mHTT) toxicity and impairs axonal trafficking, whereas overexpressing PRMT6 restores axonal transport and neuronal viability, except in the presence of a methylation-defective variant of mHTT. In HD flies, overexpressing PRMT6 rescues axonal defects and eclosion. Arginine methylation thus regulates HTT-mediated vesicular transport along the axon, and increasing HTT methylation could be of therapeutic interest for HD.

Graphical abstract

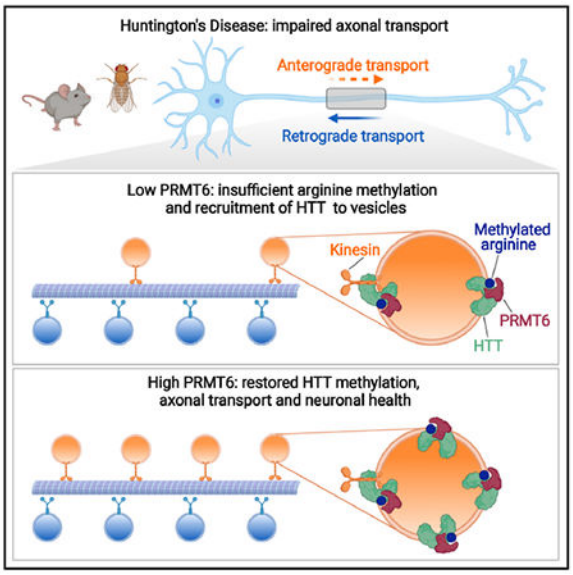

In brief

Migazzi et al. identify arginine methylation as a new post-translational modification in huntingtin (HTT) that modulates its function in axonal transport. In Huntington's disease models, enhancement of HTT methylation by PRMT6, a class I arginine methyltransferase, rescues axonal transport defects and neuronal health.

INTRODUCTION

Neuronal function depends heavily on the ability to transport various molecules along axons. Newly synthesized molecules must travel to the distal axon, while organelles and aging proteins need to return to the soma for signaling, recycling, and/or degradation. The fact that the pathogenesis of several neurodegenerative diseases involves impairments in axonal transport indicates how crucial this activity is to neuronal viability (Hinckelmann et al., 2016; Millecamps and Julien, 2013). In the case of Huntington's disease (HD), which is caused by polyglutamine expansions in the huntingtin (HTT) protein, the relationship between transport and pathogenesis is quite direct: HTT is a scaffold for both kinesin-1 and dynein motors, which drive anterograde and retrograde trafficking, respectively (Saudou and Humbert, 2016). In fact, HTT interacts with over 200 proteins, many of which are active in microtubule (MT)- or actin-based transport (Schulte and Littleton, 2011). In HD neurons, flies, and mice, however, mutant HTT (mHTT) impedes fast axonal transport (Gauthier et al., 2004; Gunawardena et al., 2003; Trushina et al., 2004) and interferes directly with the trafficking of brain-derived neurotrophic factor (BDNF) and autophagosomes (Gauthier et al., 2004; Wong and Holzbaur, 2014). Trafficking is derailed even during the very early stages of human development, disrupting neurogenesis (Barnat et al., 2020).

Post-translational modifications (PTMs) of mHTT, such as sumoylation, acetylation, and palmitoylation, influence its toxicity (Chaibva et al., 2016; Chiki et al., 2017; Jeong et al., 2009; Steffan et al., 2004; Subramaniam et al., 2009; Yanai et al., 2006), but so far, only

phosphorylation has been shown to influence HTT's interactions with motor proteins and vesicles. For example, phosphorylation of HTT at serine 421 (S421) promotes the recruitment of kinesin to BDNF vesicles, leading to anterograde flux and BDNF release (Colin et al., 2008), while its dephosphorylation promotes retrograde transport. HTT phosphorylation at S1181/S1201, on the other hand, helps motors and BDNF vesicles detach from MTs (Humbert et al., 2002; Ben M'Barek et al., 2013; Zala et al., 2008).

A proteomic study, however, raised the possibility of another kind of PTMs when it found that HTT interacts with several arginine methyltransferases (PRMTs; PRMT1, PRMT3, and PRMT5) (Ratovitski et al., 2012, 2015). PRMTs catalyze the transfer of methyl groups from S-adenosylmethionine (SAM) to the terminal nitrogen atom of the guanidinium side chain of arginine residues. HTT seems to activate PRMT5's histone-modifying activity, which plays a role in the transcriptional alterations that occur in HD (Ratovitski et al., 2015), but so far no PRMT has been shown to methylate HTT or to affect its activity. Given that arginine methylation influences protein structure and function (Blanc and Richard, 2017) and that it is particularly abundant in neurons (Guo et al., 2014), we wondered whether HTT itself is methylated by PRMTs and, if so, whether this influences HTT's roles in axonal transport.

RESULTS

HTT undergoes arginine methylation by PRMT6

To determine whether HTT is arginine methylated *in vivo*, we immunopurified HTT from vesicular fractions isolated from brains of wild-type mice and analyzed HTT arginine methylation by mass spectrometry (MS) (Figure 1A). We identified two candidate arginine (R) residues for dimethylation *in vivo*: R101 and R118 (Figures 1B and S1A). MS analysis on full-length HTT immunopurified from HEK293 cells also detected monomethylation of human HTT at R118 (Figure S1B; Table S1). R101 and R118 are very well conserved throughout evolution (Figure S1C; Tartari et al., 2008), being present in all the Deuterostomia analyzed here; R118 even appears in the unicellular organism *Dictyostelium discoideum* and in protostomes such as the nematode *Ascaris suum*.

To identify the PRMTs responsible for HTT arginine methylation, we co-expressed the N-terminal fragment of HTT corresponding to the first 548 amino acids bearing 17 glutamine residues (HTT 548-17Q) together with either soluble enhanced green fluorescent protein (EGFP) or PRMT1–PRMT8 tagged with EGFP in HEK293T cells. By immunoprecipitating the EGFP-fused PRMTs, we found that HTT 548-17Q forms a complex with PRMT2 and PMRT6 and, to a lesser extent, PRMT1, PRMT5, and PRMT7 (Figure 1C). Similar results were obtained by reverse immunoprecipitation with an antibody that recognizes HTT, confirming the interaction of HTT 548-17Q with PRMT2 and PRMT6 (Figure S1D).

To determine whether full-length HTT interacts with PRMT 2 and 6, we immunoprecipitated HTT from immortalized striatal cells expressing full-length HTT-7Q ($STHdh^{Q7/Q7}$) (Trettel et al., 2000) and confirmed its interaction with overexpressed PRMT 2 and 6 (Figure 1D). We then used an *in situ* proximity ligation assay (PLA) (Tripathy et al., 2017) to find that endogenous HTT associates with endogenous PRMT2 and PRMT6 in the nucleus as well as in the cytosol of $STHdh^{Q7/Q7}$ cells (Figures 1E and S1E).

PRMT2 and PRMT6 catalyze the formation of asymmetric dimethylarginine (ADMA). To determine whether PRMT2 and PRMT6 methylate HTT at R101 and R118, we performed an *in vitro* methylation assay by incubating wild-type or methylation-defective glutathione S-transferase (GST)-HTT fusion proteins containing R101 and R118 as the only arginines (HTT 91–144) with recombinant PRMT2 and PRMT6 and the methylation donor [^{3}H]-SAM. PRMT2 did not methylate HTT at these arginine residues in these assays, regardless of its ability to increase the levels of asymmetrically dimethylated histone H3 at arginine 8 (H3R8me2a) in test tubes (Figure S1F). PRMT6, however, modified wild-type and R101A, but not R118A HTT (Figure 1F), indicating that PRMT6 specifically methylates HTT at R118.

To determine whether PRMT6 methylates HTT in cells, we expressed HTT 548–17Q either alone or together with EGFP-PRMT6 and performed immunoprecipitation with an antibody that recognizes arginine-methylated proteins (Figure S1G). We found that overexpression of wild-type PRMT6 induced HTT arginine methylation, whereas its catalytically inactive form (PRMT6-V86K,D88A) reduced arginine methylation to 0.70 of wild-type levels. Inhibiting PRMT6 with Adox or EPZ020411 (EPZ) reduced arginine methylation to 0.74 and 0.45 of normal levels, respectively (Figure S1G). We then mutated R118 to lysine to generate a methylation-defective HTT variant, HTT-R118K. HTT 548 17Q-R118K retained the ability to form a complex with PRMT6 (Figure S1H), and its global ADMA levels were similar to those of wild-type HTT, suggesting that HTT is methylated at other arginine residues (Figure S1I).

To validate methylation of HTT by PRMT6 in neurons, we transduced primary mouse cortical neurons with HTT-548–17Q and either EGFP or EGFP-PRMT6. PRMT6 increased HTT arginine methylation 1.5-fold, but again, inhibiting PRMT6 with EPZ prevented this effect (Figure 1G). We immunoprecipitated full-length HTT from rat primary cortical neurons transduced with EGFP-PRMT6 and analyzed HTT methylation using an antibody that specifically recognizes ADMA. We found that PRMT6 asymmetrically dimethylates endogenous HTT (Figure 1H).

PRMT6 localizes to axonal vesicles

Immunofluorescence analysis showed overlapping PRMT6 and HTT punctate staining in striatal cells (Figure S2A). To determine whether HTT and PRMT6 truly share subcellular localization in primary cortical and striatal neurons, we took advantage of an *in vitro* microfluidic corticostriatal network in which cortical and striatal neurons in different compartments connect to each other through microchannels and an intermediate synaptic chamber (Virlogeux et al., 2018; Figure 2A). Airyscan confocal microscopy showed punctuate colocalization of HTT and PRMT6 in cortical and striatal neurons, and in isolated cortical axons identified by the staining with overexpressed VAMP2-mCherry (Figures 2B and 2C). The Manders' overlap coefficients (M1 and M2) were 0.49 and 0.52 in the cortex and 0.39 and 0.47 in the striatum (Figure S2B).

To determine whether the colocalization resulted in a specific interaction, we took advantage of the PLA in mouse cortical neurons. We observed that most of the interaction happened in the axons and processes (Figures 2D, S2C, and S2D). As expected, subcellular fractionation

of mouse forebrain extracts revealed both PRMT6 and HTT in the P1 (mostly nuclear proteins) and S3 (mostly cytosolic proteins) fractions. Importantly, PRMT6 was also detected in the fraction enriched in vesicle-associated proteins (P3), such as HTT and $p150^{glued}$ (Colin et al., 2008; Gauthier et al., 2004; Figure 2E). Transmission electron microscopy (TEM) coupled to immunogold staining of purified vesicles revealed PRMT6 on HTT-positive vesicles (Figures 2F and S2E). An average of ~1.3 PRMT6 molecules per vesicle was observed (Figure 2G), and, after dual staining of both HTT and PRMT6, we observed that 37% of HTT-positive vesicles contain PRMT6. The colocalization of the two proteins was more prevalent in small vesicles (<60 nm) than in large vesicles (>60 and <150 nm) (Figure 2H).

Loss of HTT R118 methylation impairs vesicle trafficking and leads to neurotoxicity

To determine whether arginine methylation affects HTT-mediated vesicular transport, we first performed videomicroscopy in neurons transduced with lentiviral constructs expressing HTT-mCherry and EGFP-PRMT6. We observed that both HTT and PRMT6 trafficked on the same vesicles in cortical axons (Figure S3A). We next transduced cortical neurons plated in the microfluidic chambers with lentiviral constructs expressing HTT 548-17Q or the methylation-defective HTT mutant (HTT 548-17Q R118K) fused to mCherry, and we recorded the trafficking of HTT-positive vesicles in the distal part of axonal microchannels to avoid dendritic contamination (Virlogeux et al., 2018; Figure 3A). Immunoblotting indicated that both HTT 548-17Q-mCherry and the methylation-defective HTT variant were expressed at similar levels and showed a similar cytosolic distribution in neurons (Figures S3B and S3C). The expression of HTT 548-17Q R118K did not alter neuronal morphology, as the number and length of neurites did not change (Figure S3D). Fast video acquisitions were performed at 12 days *in vitro* (DIV12) to DIV14, when neurons in the microchambers are already organized in a mature network with fully functional unilateral corticostriatal synapses (Virlogeux et al., 2018). Quantitative analyses found no difference in retrograde transport compared to neurons expressing methylatable HTT (Figure S3E). Neurons expressing the methylation-defective HTT, however, had 46% fewer anterograde vesicles, a lower global linear flow rate of 31%, and a shift toward retrograde trafficking (Figure 3A). We confirmed these results by silencing PRMT6 with a specific short hairpin RNA (shRNA) (Figure S3F; Scaramuzzino et al., 2015). Neurons expressing a lower level of PRMT6 showed 30% fewer anterograde vesicles, a lower global linear flow rate of 26%, and a shift toward retrograde trafficking (Figure 3B). We did not detect a difference in retrograde transport of HTT-positive vesicles upon PRMT6 silencing (Figure S3G).

To test whether the observed alteration in axonal trafficking would translate in an impaired HTT function in axonal transport, we expressed BDNF-mCherry in cortical neurons and recorded axonal trafficking. PRMT6 inhibition decreased both anterograde and retrograde velocity of 25% and 24%, respectively, and doubled the number of pausing vesicles, thereby reducing anterograde trafficking toward the synapse, as shown by the directional flux (Figures 3C and S3H). These altered BDNF transport dynamics demonstrate that a HTT's scaffolding function in axonal trafficking is influenced by PRMT6.

We next asked whether HTT arginine methylation affects HTT's interaction with kinesin and the dynein-dynactin complex. We transduced primary cortical neurons with HTT 548-17Q-mCherry and HTT 548-17Q R118K-mCherry, immunopurified HTT with anti-mCherry antibody, and analyzed interactions with the molecular motors. Both methylation-defective and wild-type HTT interacted with the p150 subunit of dynactin and kinesin heavy chain (KHC) (Figure 3D). Next, we performed a subcellular fractionation of neurons transduced with either HTT 548-17Q-mCherry or HTT 548-17Q R118K-mCherry and observed that loss of arginine methylation at R118 reduced HTT recruitment to vesicles by 40% (Figures 3E and 3F). Because defects in axonal trafficking occur in several neurodegenerative conditions (Hinckelmann et al., 2013), we asked whether the alteration in vesicular trafficking correlated with neuronal toxicity. By DIV11, overexpression of HTT-R118K-mCherry or silencing of PRMT6 reduced neuronal viability by almost 50% or 40%, respectively (Figures 3G and 3H; Tripathy et al., 2017).

Together, these results suggest that loss of arginine methylation by either PRMT6 repression or the expression of a HTT-methylation-defective mutant diminishes the presence of wild-type HTT in the vesicular fraction, reducing anterograde trafficking of HTT-positive vesicles and leading to neurotoxicity. The reduction in HTT-positive vesicles correlates with the impairment of BDNF transport toward the synapses, underscoring the importance of HTT arginine methylation for HTT function.

mHTT interacts with and is methylated by PRMT6 *in vivo*

Pull-down and PLA showed that mHTT forms a complex with PRMT6 in non-neuronal cells and in striatal cells expressing HTT-111Q ($STHdh^{Q111/Q111}$) (Figures 4A–4C). MS analysis on immunoprecipitated HTT showed that human mHTT is dimethylated at R118 (Figure 4D; Table S2). PRMT6 transcript and protein levels were similar in $STHdh^{Q7/Q7}$ and $STHdh^{Q111/Q111}$ cells (Figures S4A and S4B). We also analyzed PRMT6 protein levels in the cortex and striatum of HD patient tissues, and although the samples showed high heterogeneity, we found no significant difference between them (Figures 4E–4H; Table S3). Finally, we analyzed PRMT6 protein expression in the cortex of $Hdh^{CAG140/+}$ knockin mice at an early symptomatic stage (6 months). PRMT6 was equally expressed in knockin mice and controls (Figures S4C and S4D).

We conclude that the polyglutamine expansion does not disrupt formation of a mHTT-PRMT6 complex or methylation at R118. Moreover, PRMT6 levels are not altered in HD models. This suggests that stimulating PRMT6 activity to increase R118 methylation and HTT-mediated anterograde transport could be a viable approach to treating the trafficking defects seen in HD.

Arginine methylation mitigates mHTT neurotoxicity and axonal defects in neurons

To assess whether R118 methylation influences neurotoxicity in HD, we first analyzed cell viability in STHdh cells after PRMT6 knockdown. We transduced striatal cells with lentiviral vectors expressing either a scramble shRNA or an shRNA against PRMT6 (Scaramuzzino et al., 2015). The shRNA against PRMT6 lowered its mRNA transcript levels by 45%–80% in $STHdh^{Q7/Q7}$ and $STHdh^{Q111/Q111}$ cells and its protein levels by ~50%

(Figures S5A and S5B). Knockdown of PRMT6 reduced survival of STHdh$^{Q7/Q7}$ cells by 27%, but survival of STHdh$^{Q111/Q111}$ cells was reduced by nearly half (47%) (Figures 5A, S5C, and S8). We then transduced cultured primary cortical neurons with lentiviruses expressing HTT fragments with an expanded polyglutamine tract (HTT 548-73Q fused with mCherry) together with a scramble or a PRMT6 shRNA. PRMT6 silencing in cortical neurons resulted in 50% neuronal loss (Figure 5B). To validate the specific impact of PRMT6 in HD, we silenced PRMT2, which interacted with but did not methylate HTT (Figure 1C). The shRNA against PRMT2 decreased mRNA transcript levels by 80% in STHdh$^{Q7/Q7}$ and STHdh$^{Q111/Q111}$ cells (Figure S5D), but knockdown of PRMT2 did not reduce cell survival (Figure S5E). Loss of PRMT6-mediated HTT arginine methylation thus clearly exacerbated toxicity in striatal cells and cortical neurons expressing mHTT.

We then transduced cultured primary cortical neurons with lentiviruses expressing either HTT 548-73Q-mCherry or a methylation-defective HTT 548-73Q R118K-mCherry (Figure S5F) under the synapsin I promoter (Tripathy et al., 2017). Expression of mHTT and the methylation-defective mHTT reduced neuronal viability by 31% and 38%, respectively, as compared to control neurons expressing HTT 548-17Q (dotted line, Figure 5C). PRMT6 overexpression rescued neuronal death caused by mHTT, but this rescue was prevented by methylation-defective mHTT (Figure 5C). When overexpressed, PRMT6 accumulated on vesicles (P3 fraction) (Figure S5G) and significantly increased the efficiency of anterograde trafficking in neurons expressing mHTT, but not those expressing methylation-defective mHTT (Figure 5D). As we observed with overexpression of the arginine mHTT, PRMT6 silencing did not exacerbate the trafficking defect observed when only HTT 548-73Q was overexpressed together with a scramble shRNA (Figure 5D). HTT methylation at R118 is therefore necessary for PRMT6 to improve axonal transport and viability in HD neurons *in vitro*.

To investigate how PRMT6 promotes axonal transport in HD cells, we performed a subcellular fractionation of heterozygous STHdh$^{Q7/Q111}$ transduced with either EGFP or EGFP-PRMT6. PRMT6 overexpression increased the amount of wild-type HTT being recruited to vesicles by 130% but had no effect on the level of mHTT in the vesicular fraction (Figures 5E and 5F). These data suggest that increasing methylation rescues axonal transport and reduces neuronal death by displacing mHTT on vesicles in favor of wild-type HTT (i.e., by enhancing the recruitment of wild-type HTT to vesicles).

Arginine methylation rescues eclosion, axonal transport, and neuromuscular junction (NMJ) defects in fly model of HD

To investigate whether augmenting PRMT6 expression abrogates mHTT-induced toxicity *in vivo*, we used a *Drosophila* HD model expressing HTT with 128 glutamine residues in neurons (HTT-128Q) (Figure 5G). We used the inducible pan neuronal GeneSwitch system (Osterwalder et al., 2001) and evaluated pupal eclosion upon crossing HD flies with flies that overexpress PRMT6 (Scaramuzzino et al., 2015). As previously reported (Scaramuzzino et al., 2015), PRMT6 overexpression in flies did not produce any overt phenotype. Expression of HTT-128Q prevented fly eclosion, but overexpression of PRMT6 rescued eclosion. Gain of PRMT6 function *in vivo* thus mitigates mHTT toxicity.

To address whether expression of PRMT6 rescues HTT-mediated axonal transport and NMJ defects *in vivo*, we targeted the expression of HTT 128Q and PRMT6 in *Drosophila* neurons using the ELAV-GeneSwitch system (Anderson et al., 2018). To assess axonal accumulations, we stained larval segmental nerves from control flies and flies expressing PRMT6, HTT 128Q, or PRMT6/PRMT6 HTT 128Q with the synaptic vesicle protein cysteine string protein (CSP), a marker frequently used to reveal axonal transport defects (Gunawardena and Goldstein, 2001). CSP accumulations are called axonal blockages and are observed in fixed or live segmental nerves (Gindhart et al., 1998; Gunawardena and Goldstein, 2001; Gunawardena et al., 2003). Expression of HTT 128Q led to accumulation of CSP in segmental nerves compared to controls, which showed smooth CSP staining (Figure 6A).PRMT6 overexpression markedly reduced the number of CSP blocks caused by HTT 128Q expression (Figure 6B). Confocal microscopy of flies expressing HTT 128Q showed no difference in the number of mature boutons (Figure 6D) but a dramatic increase in the number of satellite boutons (those that bud off mature boutons) (Figure 6C, arrowheads) and total boutons (Figures 6E and 6F). These numbers were restored to control levels by PRMT6 overexpression (Figures 6E and 6F). PRMT6 thus rescues morphological defects at the NMJ as well as axonal transport defects *in vivo*.

DISCUSSION

Arginine methylation has been much less studied than phosphorylation and acetylation, but recent work has shown that it is involved in at least two neurodegenerative proteopathies. In spinal and bulbar muscular atrophy (SBMA), which is caused by polyglutamine expansions in the gene coding for the androgen receptor (AR), arginine methylation of mutant AR augments its native function and exacerbates neuronal toxicity (Basso and Pennuto, 2015; Scaramuzzino et al., 2015). In fly models of amyotrophic lateral sclerosis (ALS), loss of arginine methylation in the DNA/RNA-binding protein fused in sarcoma (FUS) (Vance et al., 2009) leads to neurodegeneration (Hofweber et al., 2018; Qamar et al., 2018; Scaramuzzino et al., 2013), perhaps because of loss of the ability to degrade stress granules by a complex containing C9orf72 and the autophagy receptor p62 (Chitiprolu et al., 2018). Finally, the protein survival motor neuron (SMN), whose loss of function is involved in spinal muscular atrophy, has a Tudor domain that binds dimethylated proteins, such as RNA polymerase II and the Sm proteins, to coordinate gene transcription termination and biogenesis of small nuclear ribonucleoproteins (Friesen et al., 2001; Zhao et al., 2016). Loss of methylation in these proteins alters SMN function and reproduces the transcriptional defects observed in SMA patients (Zhao et al., 2016); one study in SMA patient motor neurons found SMN's interaction with the spliceosome through the Tudor domain impaired, resulting in a reduction in Cajal bodies (Tapia et al., 2012). These studies lend support to the notion that changes in arginine methylation, or the ability to "read" it, are crucial to neuronal function. What is unprecedented here is the finding that arginine methylation helps regulate axonal transport through its influence on HTT function.

The transport of cargos by motor proteins along MTs is influenced by several mechanisms (Maday et al., 2014). These include phosphorylation of MTs (Magiera et al., 2018) or MT-associated proteins such as Tau (Wang et al., 2013) that indirectly affect the activity of motor proteins. Other modifications such as acetylation increase the affinity of the motors to MTs

and thus reduce neurodegeneration (Dompierre et al., 2007). The activity of motor proteins can also be directly regulated by PTMs. For example, kinesin-1 is phosphorylated by kinases such as JNK3, leading to a reduction in its processivity on MTs and thereby diminishing transport efficacy (Morfini et al., 2016). Another level of regulation lies with molecular motor adaptors such as JIP1 and HTT, which play an important role in modulating the recruitment or the activity of molecular motors (Maday et al., 2014; Saudou and Humbert, 2016). Interestingly, kinases such as CDK5, JNK, and Akt and phosphatases such as calcineurin or MKP1 regulate the phosphorylation state of scaffold/ adaptor proteins like JIP1 and HTT and either recruit motors or change their activity, but the exact mechanisms by which phosphorylation of scaffold proteins modulates axonal trafficking have not yet been fully elucidated (Fu and Holzbaur, 2014; Klinman et al., 2017; Morfini et al., 2009).

In the case of HTT, different mechanisms regulate transport efficiency, either by recruiting specific motors on vesicles or by increasing the attachment of vesicles and their motors to MTs. For example, phosphorylation by Akt at S421 leads to the recruitment of kinesin-1 to the complex, promoting anterograde transport (Colin et al., 2008), whereas phosphorylation by CDK5 reduces attachment of vesicles and motors to MTs (Ben M'Barek et al., 2013). In the present study, we observed no difference in the interaction between kinesin-1 and dynein and the methylation-defective HTT, indicating that arginine methylation does not alter motor-HTT interactions. We did, however, observe less HTT in the vesicular fraction, which suggests that arginine methylation helps HTT bind vesicles and that HTT stoichiometry on the vesicle affects its scaffolding function and therefore axonal transport. How HTT is recruited to vesicles, and which intracellular signal drives methylation at the vesicular level, are currently unknown, but our data suggest that methylation could be part of this mechanism. It remains to be seen whether other components of the motor complex are arginine methylated or contain a Tudor domain that recognizes methylarginines.

Methylation by PRMTs has usually been associated with histone proteins, transcription factors, RNA-binding proteins, and factors regulating splicing (Basso and Pennuto, 2015; Blanc and Richard, 2017; Guccione and Richard, 2019), but it has not been previously found to be involved in axonal transport. Our TEM showed that PRMT6 and HTT both reside on the external vesicular surface, suggesting that PRMT6-mediated methylation of HTT initiates a signaling cascade that facilitates the latter's function in axonal trafficking. In a similar vein, PRMT1 methylation of Smad4 activates Wnt signaling, which stimulates endosomes to mature in multivesicular bodies and fuse with lysosomes via microautophagy (Albrecht et al., 2018). Our data suggest that the presence of PRMT6 on vesicles facilitates HTT's function as a scaffold of molecular motors and promotes the anterograde movement of the motor complex on MTs. This is consistent with a model we previously proposed in which neuronal motile vesicles possess all the enzymes required to self-fuel their axonal transport (Hinckelmann et al., 2016; Zala et al., 2013).

One question raised by our results is the identity of arginine demethylases that remove methyl groups from arginine residues (Blanc and Richard, 2017; Wesche et al., 2017). Such demethylases might help HTT release the vesicle or the motor. Jumonji-domain-containing protein 6 (Jmjd6) was the first putative arginine demethylase to be identified (Chang et al., 2007), but its enzymatic activity was later questioned by several groups (Hahn et al., 2010;

Wang et al., 2014; Webby et al., 2009) and is still debated. Similarly, it was proposed that the peptidyl arginine deiminase PAD4 could convert methylated arginines to citrulline (Thompson and Fast, 2006; Wang et al., 2004), but citrullination and arginine methylation are now considered competing PTMs (Fuhrmann and Thompson, 2016; Wesche et al., 2017). Some lysine demethylases (KDMs) can catalyze arginine demethylation *in vitro,* but this has not been investigated in living cells (Blanc and Richard, 2017; Wesche et al., 2017). Nonetheless, several studies show dynamic changes in arginine methylation marks, strongly suggesting that arginine methylation is a reversible PTM (Wesche et al., 2017). It is thus very likely that enzymes with specific arginine demethylase activity will be identified. In this scenario, PRMT6 localization on vesicles would be key to reverse the activity of arginine demethylases and ensure tight regulation of the arginine methylation status of vesicle-associated HTT.

Our results also imply that inhibition of arginine methylation could contribute to HD pathogenesis. We found that PRMT6 is expressed at similar levels in the brains of HD patients and healthy controls and that arginine methylation of mHTT is preserved, but S-adenosylhomocysteine hydrolase (SAHH), the enzyme that catalyzes the hydrolysis of S-adenosylhomocysteine (SAH) to adenosine and homocysteine, is downregulated in the striatum of transgenic HD mice and peripheral leukocytes of HD patients (Chang et al., 2012). By negative feedback, SAH strongly inhibits SAM-dependent methyltransferases, including PRMTs (Baric et al., 2004), and abnormally high levels of SAH or an imbalance of SAM/SAH in neurons could therefore suppress PRMT6 enzymatic activity in HD patients, effectively reducing HTT methylation. Interestingly, the methionine cycle that produces the methyl-donor SAM and the transulfuration pathway that yields cysteine in the cells are interconnected, along with a third cycle that utilizes folate and B vitamins in the one-carbon cycle (Locasale, 2013). Snyder and colleagues reported that HD tissues are depleted in the biosynthetic enzyme for cysteine, cystathionine γ-lyase (CSE), which leads to oxidative stress and thereby contributes to HD pathogenesis (Paul et al., 2014). They also showed that cysteine supplementation delays neurodegeneration in the R6/2 mouse model of HD (Paul et al., 2014). Our study identifies arginine methylation as a regulator of HTT function in axonal transport and further supports the hypothesis that imbalance of several metabolites of the one-carbon cycle might be involved in HD pathophysiology. The reversal of HD-related changes we observed in cultured neurons and the HD fly model with PRMT6 overexpression suggests that global stimulation of the one-carbon metabolism that provides the methyl-donor SAM could be of therapeutic interest in HD.

STAR★METHODS

RESOURCE AVAILABILITY

Lead contact—Further information and requests for resources and reagents should be directed to and will be fulfilled by the Lead Contact, Manuela Basso.

Materials availability—Newly generated plasmids are available upon request.

Data and code availability—This study did not generate datasets.

EXPERIMENTAL MODEL AND SUBJECT DETAILS

Animals—Animal care and experimental procedures were conducted in accordance with the Ethical Committee of the University of Trento and were approved by the Italian Ministry of Health (D. Lgs no. 2014/26, implementation of the 2010/63/UE). Animals were maintained with access to food and water *ad libitum* and kept at a constant temperature (19–22°C) on a 12:12 h light/dark cycle. Primary mouse cortical neurons were obtained from wild-type C57BL/6J mice (Charles River Laboratories, Italy) mated to generate male and female embryos.

For our HD mouse model, we used 6 months-old $Hdh^{CAG140/+}$ heterozygous knock-in mice generated on a C57BL/6J background, which express the human HTT exon 1 sequence with 140 CAG repeats, as previously described (Virlogeux et al., 2018). All experimental procedures were performed in an authorized establishment (Institut des Neurosciences de Grenoble (GIN), U1216, license #B3851610008) in strict accordance with the local animal welfare committee (Comité Local Grenoble Institut Neurosciences, C2EA-04) and the EU guidelines (directive 63/2010/EU) on the protection of animals used for experimental research.

Cell lines—HEK293T cells were maintained in DMEM supplemented with 10% fetal bovine serum, L-Glutamine (2 mM) and PenStrep (1%) and grown at 37°C with 5% CO_2. Immortalized striatal cells (STHdh; Trettel et al., 2000) were maintained in DMEM supplemented with 10% fetal bovine serum, L-Glutamine (2 mM), sodium pyruvate (1 mM), G418 (0.4 mg/ml) and grown at 33°C with 5% CO_2 until passage 14. We kindly received the $STHdh^{Q7/Q7}$ (clone 2a1) and the $STHdh^{Q111/Q111}$ (clone 109.1) from Dr. Marcy E. MacDonald.

Flies—All *Drosophila* stocks were maintained on standard cornmeal medium at 28°C in light/dark-controlled incubators. The ELAV-GeneSwitch (ElavGS), w1118 (CTRL), and UAS-HTT16Q UAS-HTT128Q were obtained from Bloomington stock center. The UAS-PRMT6 was generated through site-specific integration of the transgene at BestGene Inc. using the (attP2) insertion vector. Both males and females were used for the assays. The NMJ analysis was performed on the 3^{rd} instar larvae and we monitored the emergence of the adult flies (day 1) from the pupal case.

Human subjects—We obtained post-mortem specimens of frontal cortex and striatum from subjects with HD and control subjects from the Institute of Neuropathology (HUB-ICO-IDIBELL) Brain Bank (Hospitalet de Llobregat, Spain)/Neurological Tissue Bank of the IDIBAPS Biobank (Barcelona, Spain) and the Banco de Tejidos Fundacion Cien (BT-CIEN, Madrid, Spain). Specimens from both male and female subjects were used for the western blotting analysis. The age and sex of the human subjects is described in Table S3. The donors and/or next of kin provided written informed consent for brain removal after death for diagnostic and research purposes. Procedures, information and consent forms have been approved by the Bioethics Subcommittee of Centro Superior de Investigaciones Cientificas (Madrid, Spain).

METHOD DETAILS

Purification of vesicle-associated HTT and mass spectrometry analysis—The subcellular fractionation was performed as previously described (Hinckelmann et al., 2016). Briefly, mouse brains were collected and mechanically homogenized in lysis buffer (4 mM HEPES, 320 mM sucrose pH 7.4) containing protease inhibitor (Sigma Aldrich-P8340) and phosphatase inhibitor (Sigma Aldrich #P5726) cocktails. The homogenate was subjected to sequential centrifugation steps (Figure 1A) to isolate the small vesicles-rich fraction (P3), which was resuspended in lysis buffer. To select vesicle-associated HTT, the P3 fraction (1 mg) was pre-cleared for 1 hour at 4°C with Protein A Sepharose beads (Sigma Aldrich #P9424) and subjected to immunoprecipitation on a rotating wheel for 3 hours at 4°C with agarose beads pre-incubated with 2,5 μg anti-HTT D7F7 antibody (Cell Signaling #5656). The beads were washed three times in lysis buffer and proteins were eluted with Laemmli buffer and boiled at 95°C for 10 min. After SDS-PAGE, the band corresponding to HTT was cut and analyzed by LC-MS/MS to identify HTT post-translational modifications (PTMs). MS was performed with a LTQ Orbitrap XL mass spectrometer (Thermo Scientific), equipped with a nanoESI source (Proxeon). The top eight peaks in the mass spectra (Orbitrap; resolution, 60,000) were selected for fragmentation (CID; normalized collision energy, 35%; activation time, 30 ms, q-value, 0.25). Dynamic exclusion was enabled (repeat count, 2; repeat duration, 10 s; exclusion duration, 20 s). MS/MS spectra were acquired in the LTQ in centroid mode. Proteins were identified using the MaxQuant software package version 1.2.2.5 (MPI for Biochemistry, Germany) and UniProt database version 04/2013.

Purification of HTT from transfected HEK293 cells and mass spectrometry analysis—HEK293 cells were transfected with full-length human normal (22Q) and expanded (82Q) HTT constructs (described in (Arbez et al., 2017)) using Lipofectamine 2000 reagent (ThermoFisher). 24h post transfection cells were lysed by the Dounce homogenization in Triton lysis buffer containing 50 mM Tris, pH 7.0,150 mM NaCl, 5 mM EDTA, 50 mM $MgCl_2$, 0.5% Triton X-100, 0.5% Na deoxycholate, Protease Inhibitor Cocktail III (Calbiochem), and Halt Phosphatase Inhibitor Cocktail (ThermoFisher), followed by centrifugation at 13,000 g. Lysates were pre-cleared by incubating with Protein G-Sepharose beads (GE Healthcare) for 1 h at 4°C, followed by incubation overnight at 4°C with the primary anti-HTT antibody (MAB2166, Millipore) to IP normal HTT, or with MW1 polyQ-specific antibody (Hybridoma Bank, University of Iowa) to IP expanded HTT. These were then incubated with Protein G-Sepharose for 1 h at 4°C. The IPs were washed 3 times with the lysis buffer, and HTT proteins were eluted from the beads with heating (80°C) in 2×SDS Laemmli sample buffer (BioRad), followed by fractionation on NuPAGE 4%–12% Bis-Tris polyacrylamide gels (ThermoFisher). HTT protein bands were visualized with SimplyBlue Safe Stain (ThermoFisher). Aliquots (about 10% of the sample) were analyzed by western blotting with antibodies to HTT (Millipore #MAB2166) and polyQ-specific antibody MW1. Normal and polyQ-expanded HTT protein bands were cut out of the gel, subjected to in-gel digestion with LysC and analyzed by tandem mass spectrometry (MS) on the Q-Exactive mass spectrometer as described previously (Ratovitski et al., 2017).

Plasmids—The vector for the expression of wild-type human N-terminal HTT (pCAG 17Q HTT-N548) was obtained from the laboratory of E. Cattaneo (University of Milan, Italy).

pCAG 73Q HTT-548 was obtained by cloning of the fragment containing the polyCAG tract from vectors expressing full-length human HTT (Coriell Institute #CH00023). For the production of recombinant GST-HTT fusion proteins, HTT sequence comprised between amino acids 91 and 144 (HTT 91-144) was subcloned into pGEX-6P-3 plasmid downstream of glutathione-S-transferase (GST) and PreScission™ Protease sequences using the following primers: Fwd CAGAGGATCCCCAAA-GAAAGAACTTTCAGC; Rev: TCTGCTCGAGCTAGACATCTGACTCTGCGTC, containing BamHI and XhoI restriction sites at the 5′ and 3′, respectively. Methylation-defective arginine-to-alanine GST-HTT mutants were obtained by site-directed mutagenesis PCR using the following forward (F) and reverse (R) primers: R101A-F, 5′-TCAGCTACCAAGAAAGACGCTGTGA-3′; R101A-R, 5′-TGTCAGACAATGATTCACAGCGTCT-3′; R118A-F, 5′-ATAGTGGCACAGTCTGTCGCAAATTC-3′; R118A-R, 5′-CTGAAATTCTGG AGAATTTGCGACA-3′. All constructs were confirmed by sequencing. To generate HTT-548-mCherry constructs, HTT 548 sequence was amplified by PCR with primers containing KpnI and BamHI restriction sites at the 5′ and 3′, respectively (Fwd: CAGAGGTACC CCACCATGGCGACCCTG; Rev: CCATCTGACCCTGCCGGGATCCCAGA), and cloned upstream of mCherry sequence in pCDNA3.1-mCherry vector (the stop codon was substituted by a glycine residue). For toxicity experiments in primary neurons, HTT-548-mCherry sequences were then cloned into HpaI and EcoRI restriction sites of the LentiLox 3.7 backbone under the control of the neuron-specific synapsin I promoter (Tripathy et al., 2017), using the following primers for the PCR: Fwd CAGAGTTAACCA CCATGGCGACC; Rev TCTGGAATTCTTACTTGTACAGCTC. Methylation-defective arginine-to-lysine HTT mutants were obtained by site-directed mutagenesis PCR using the following forward (F) and reverse (R) primers: R118K-F, 5′-ATAGTGGCACAGTCTGTCAAGAATTC-3′; R118K-R, 5′-CTGAAATTCTGGAGAATTCTTGACA-3′. All constructs were confirmed by sequencing.

For the expression of EGFP-PRMT6 in primary neurons, EGFP-PRMT6 sequence was cloned downstream of synapsin I promoter in the LentiLox 3.7 backbone described above using primers containing HpaI and EcoRI restriction sites at the 5′ and 3′, respectively (Fwd: CAGAGTTAACCACCATGGTGAGCAA; Rev: TCTGGAATTCTCAGTCCTCCAT).

PRMT2 shRNA constructs (in pGFP-C-shLenti vector) were purchased from Origene (cat. No. TL500997), whereas lentiviral constructs (pLKO.1-puro) for shRNA against PRMT6 and the corresponding scramble were kindly provided by Ernesto Guccione (Phalke et al., 2012). Both contain a puromycin resistance cassette. The most efficient knock-down was observed with PRMT2 shRNA TL500997D and shPRMT6 #1 (CACCGGCATTCTGAGCATCTT). STHdh clones expressing these shRNAs were used for the assessment of toxicity.

Cell lines, transfection, and generation of stable clones—HEK293T cells were maintained in DMEM supplemented with 10% fetal bovine serum, L-Glutamine (2 mM) and PenStrep (1%) and grown at 37°C with 5% CO_2. Immortalized striatal cells (STHdh, (Trettel et al., 2000)) were maintained in DMEM supplemented with 10% fetal bovine serum, L-Glutamine (2 mM), sodium pyruvate (1 mM), G418 (0,4 mg/ml) and grown at 33°C with 5%

CO_2 until passage 14. The STHdh$^{Q7/Q7}$ (clone 2a1) and the STHdh$^{Q111/Q111}$ (clone 109.1) were given to us by Dr. Marcy E. MacDonald.

HEK293T cells were transfected with polyethylenimine (PEI), whereas STHdh cells were electroporated using Amaxa Nucleofector (Lonza).

Stable STHdh single-cell clones were generated by transduction at multiplicity of infection (MOI) 10 or 20 with lentiviruses expressing either scramble or shRNA against mouse PRMT2 or PRMT6, followed by selection with puromycin (1,5 μg/ml for STHdh Q7/Q7 and 2,5 μg/ml for STHdh Q111/Q111, respectively) and dilution cloning in 96-well tissue culture plates to isolate individual cells.

Immunoprecipitation assays—All immunoprecipitation procedures were carried out at 4°C. HEK293T and STHdh cells were washed with ice-cold PBS and lysed in IP buffer (50 mM HEPES, 250 mM NaCl, 5 mM EDTA, 0.1% NP-40) plus protease inhibitors. Lysates were homogenized and cleared through 22G and 25G needles and kept on ice for 45 min. After 30 min centrifugation at 13200 rpm, the protein concentration was assessed and equal amounts of proteins for each sample were incubated overnight with the indicated antibody (anti-HTT: Merck-Millipore #MAB2166; anti-GFP: Roche #11814460001; anti-mono- and dimethylarginine: Abcam #ab412). The samples were then incubated with 30 μl of Protein A/G Plus Agarose beads (Santa Cruz, sc-2003) for 2h.

Rat and mouse cortical neurons transduced with HTT-mCherry and EGFP/EGFP-PRMT6 lentiviral constructs were lysed in IP buffer (50 mM Tris-HCl pH 7.5,137 mM NaCl, 10 mM MgCl2,10% Glycerol, 1% Triton X-100) containing protease inhibitor cocktail (Sigma-Aldrich). Neuronal lysates were pre-cleared with Sepharose 4B Fast Flow beads (Sigma-Aldrich) or Protein A/G Plus Agarose beads (Santa Cruz, sc-2003), respectively, for 3h under rotation. For the general inhibition of PRMTs and the specific inhibition of PRMT6, cells were incubated for 24h with 10 μM Adenosine-2′,3′-dialdehyde (Adox, Sigma #A7154) or 10 μM EPZ020411 (MedChemExpress #HY-12970A), respectively.

The primary antibody (anti-HTT: Merck-Millipore #MAB2166; anti-mCherry: Institute Curie Cat#A-P-R#13; anti-mono- and dimethylarginine: Abcam #ab412) was incubated with Sepharose beads for 3h and then the pre-cleared lysates were added and incubated overnight under rotation.

For all co-immunoprecipitation assays, after incubation with the primary antibodies and the beads, the samples were washed three times in cold IP buffer, resuspended in 2X SDS sample buffer, boiled for 5 min at 95°C and subjected to SDS-PAGE and immunoblotting.

Western blotting—For western blotting, cells were lysed 24-48 hours post-transfection using 1% Triton lysis buffer (25 mM Tris-HCl pH 7.4, 100 mM NaCl, 1 mM EGTA, 1% Triton X-100) or RIPA buffer (50 mM Tris-HCl pH 8.0, 150 mM NaCl, 1% NP-40, 0,5% Na-deoxycholate, 2% SDS) plus protease inhibitors. For the analysis of PRMT6 expression in WT and Hdh$^{CAG140/+}$ mice, whole brain or dissected cortex and striatum were lysed immediately after dissection in HEPES/sucrose buffer (320 mM sucrose, 4 mM HEPES pH 7.4), using a Dounce homogenizer, triturated with the pipette and finally homogenized by

several passages through a 2.5G syringe needle. Samples from human brain were stored at −80°C and ground with a mortar in a frozen environment with liquid nitrogen to prevent thawing of the samples.

For the analysis of PRMT6 expression in control and HD human samples, protein extracts were prepared by homogenizing the resulting powder in ice-cold extraction buffer (20 mM HEPES pH 7.4, 100mM NaCl, 20 mM NaF, 1% Triton X-100, 1 mM sodium orthovanadate, 1 μM okadaic acid, 5 mM sodium pyrophosphate, 30 mM β-glycerophosphate, 5 mM EDTA, protease inhibitors (Complete, Roche, Cat. No 11697498001)). Homogenates were centrifuged at 15000 rpm for 15 min at 4°C. Protein extracts were denatured at 95°C for 5 minutes and then subjected to SDS-PAGE. Proteins were transferred onto nitrocellulose membranes and blocked in 5% non-fat milk or BSA in TBS buffer, 0.1% Tween. Primary antibodies were incubated for 1h at room temperature or alternatively overnight at 4°C. InfraRed dye-conjugated (LI-COR Biosciences) or HRP-conjugated secondary antibodies were incubated for 1h at room temperature (1:10000 dilution in blocking solution) and signals were detected with an Odyssey infrared imaging system (LI-COR Biosciences) or Chemidoc™ (Bio-Rad), respectively.

The following primary antibodies were used: anti-HTT (Merck-Millipore #MAB2166,1:1000), anti-GFP (Life Technologies #A10262, 1:1000), anti-tubulin (Sigma #T7816, 1:10000), anti-mCherry (Life Technologies #PA5-34974, 1:2500), anti-PRMT6 (Bethyl Laboratories #A300-929A, 1:1000; Proteintech #15395-1-AP, 1:1000; Abcam #ab47244, 1:1000), anti-asymmetric dimethylarginine (Millipore #07-414, 1:250), anti-mono and dimethylarginine (Abcam #ab412, 1:500), anti-p150 (BD Transduction Laboratories #610474, 1:1000), anti-KHC (Covance #MMS-188P, SUK4, 1:1000), anti-GM130 (Abcam #ab52649, 1:1000; BD Transduction Laboratories #610822, 1:1000), anti-Lamin B1 (Abcam #16048, 1:1000; Abcam #133741, 1:1000), anti-calnexin (Enzo #ADI-SPA-860F, 1:1000; Sigma #C4731, 1:1000), anti-histone H3 (Genetex #GTX122148, 1:5000), anti-PRMT2 (Abcam #ab66763 1:1000), anti-H3R8me2a (Active Motif #39651,1:500). Quantifications were performed using ImageJ 1.52 software.

Immunocytochemistry—STHdh cells and primary cortical neurons were grown on poly-D-Lysine-coated coverslips. Cells were fixed with 4% paraformaldehyde for 15–20 min at room temperature. Cells were permeabilized with 0.1% Triton X-100 (in phosphate buffered saline, PBS), blocked with PBS containing 10% FBS and 0.05% Triton X-100 for 1h at room temperature. Primary antibodies were incubated overnight at 4°C in blocking solution with the following dilutions: HTT (Merck-Millipore #MAB2166, 1:100), PRMT2 (Abcam #ab66763, 1:100), PRMT6 (Abcam #ab47244, 1:100), mCherry (Life Technologies #PA5-34974, 1:600), MAP2 (Abcam #ab11267, 1:500 or Merck-Millipore #AB15452, 1:100), GFP (Merck-Millipore #MAB2510, 1:1000). The next day, after three washes with PBS, Alexa Fluor conjugated secondary antibodies (1:1000) were incubated for 1h at room temperature in the dark. The coverslips were then washed three times with PBS, incubated with Hoechst (Sigma #B2261) diluted in PBS for 10 min and mounted on glass slides with ProLong Diamond Antifade Mountant (Life technologies #P36961). Primary neurons and STHdh slides were imaged with a 63x oil-immersion objective using the Zeiss Axio

Observer Z1 inverted microscope or an inverted confocal microscope (LSM 710, Zeiss) coupled to an Airyscan detector, respectively.

***In situ* proximity ligation assay (PLA)—**The Duolink starter kit (Sigma-Aldrich #DUO92101) was used to study the interaction of endogenous HTT with endogenous PRMT2/PRMT6 in STHdh cells and cortical neurons. The assay was performed following manufacturer's instructions. Primary antibodies were incubated with the same dilutions used for immunocytochemistry experiments. Slides were imaged with the Zeiss Axio Observer Z1 inverted microscope and a 63x oil-immersion objective. For phase-contrast imaging of neurons, the acquisitions were performed by using a Leica DMi8 full motorized inverted microscope equipped with an Andor Zyla sCMOS camera (full frame 2048 pixel x 2048 pixel, 12 bit, readout frequency: 540MHz) and a HC PL Apo CS2 63x/1.40 OIL UV objective. The exposure times used were: 100 ms for both Phase contrast and Texas Red (filter set: Y3), 10 ms for DAPI acquisitions (filter set: LED 405).

Expression and purification of recombinant GST-HTT proteins—E.*coli* Rosetta (DE3) competent cells were transformed with pGEX-6P-3 plasmids coding for wild-type or mutant GST-HTT 91-144. An overnight culture grown at 37°C in LB supplemented with antibiotics was diluted into LB and grown at 37°C till OD 0.6. Protein expression was induced by the addition of 1 mM IPTG and the culture was grown overnight at 20°C. Bacteria were centrifuged at 4000 rpm for 20 min at 4°C, bacterial pellets were frozen at −80°C and subsequently resuspended in equilibration buffer (50 mM Tris, 150 mM NaCl, pH 8.0) containing protease inhibitors (cOmplete Protease Inhibitor Cocktail and PMSF). Bacterial lysis was achieved upon incubation of the resuspended pellet with lysozyme and DNase I for 1h at 4°C under agitation. Bacterial lysates were sonicated (6 cycles, 30'' ON-1' OFF) and cleared by centrifugation at 20000 rpm for 45 min. GST-HTT fusion proteins were purified by batch method using Pierce® Glutathione Agarose resin (Thermo Scientific #16100) and following manufactures's instructions. Briefly, lysates were incubated with the equilibrated resin for 1h at 4°C on an end-over-end rotator and washed three times in equilibration buffer by centrifugating for 2 min at 700 g between washes. GST-HTT proteins were eluted in two steps in equilibration buffer supplemented with 10 mM and 50 mM reduced glutathione. Protein samples were then dialyzed overnight, concentrated using Vivaspin 6 tubes (Sartorius 5,000 MWCO PES #VS0611), quantified by UV absorbance, aliquoted and flash-frozen in liquid nitrogen.

***In vitro* methylation assays—**Purified GST-HTT proteins (1.5 μg) were incubated for 3h at 37°C with 500 ng of human recombinant PRMTs (PRMT2: Active Motif #31392; PRMT6: Active Motif #31394) in the presence of 5 μCi of S-adenosyl-L-[methyl-3H] methionine (PerkinElmer) in the recommended buffer (50 mM Tris-HCl pH 8.6, 0.02% Triton X-100, 2 mM $MgCl_2$,1 mM TCEP). Samples were denatured at 95°C for 5 min and subjected to 4%–15% SDS-PAGE and Coomassie Brilliant Blue (CBB) staining. After overnight destaining, the gel was incubated for 1h with En3Hance (PerkinElmer), washed in cold water containing 3% glycerol for 30 min and dried for 3h at 80°C. The dried gel was exposed to film at −80°C for one to three weeks.

For the *in vitro* methylation assay with histone H3, 1 μg human Histone 3.1 (NEB # M2503S) was incubated for 3h at 37°C with 15 ng/μl or 30 ng/μl human recombinant PRMT2 in the recommended buffer (50 mM Tris-HCl pH 8.6, 0.02% Triton X-100, 2 mM $MgCl_2$, 1 mM TCEP, 50 μM SAM (Sigma #A7007)). Samples were denatured at 95°C for 5 minutes and analyzed by 15% SDS-PAGE and immunoblotting with anti-PRMT2, anti-histone H3 and anti-H3R8me2a primary antibodies as described above.

Primary cortical neurons—For viability assays, primary cortical neurons were cultured from E15.5 C57BL/6J mouse embryos as previously described (Basso et al., 2012). Briefly, the cortices were dissected out of the embryos, digested in papain solution (20 U papain, 500 μM EDTA and 100 μM L-cystine in 1X Eagles' Balanced Salt Solution (EBSS), Sigma #E7510) for 20 min. This was followed by DNase I treatment for 3 min. The dissociated cells were centrifuged at 2800 rpm for 5 min. The supernatant was discarded, and the digestion was blocked with a solution containing Trypsin inhibitor (Sigma T9253) and bovine serum albumin (Sigma A7030) in 1X EBSS. After a centrifugation at 2800 rpm for 10 min, the cells were seeded in poly-D-lysine-coated plates in Minimum Essential Media (MEM) supplemented with 10% fetal bovine serum, L-Glutamine (2 mM) and PenStrep (1%). Neurons were transduced at DIV0–2 at MOI 3. The day after, the medium was replaced with Neurobasal medium supplemented with B27, sodium pyruvate (1 mM), PenStrep (1%), L-Glutamine (2 mM) and AraC (100 mM, Sigma C1768). Half of the media was replaced with fresh media every 7 days. For immunoprecipitation and subcellular fractionation experiments, primary cortical neurons from E17.5 rat embryos were prepared as previously described (Virlogeux et al., 2018).

Viral production and titration—HTT-mCherry, VAMP2-mCherry, BDNF-mCherry, shPRMT6 or EGFP-PRMT6 lentiviral vectors together with psPAX2 plasmid containing *gag, pol* and *rev* genes and pMD2.G (VSV-G envelope-expressing plasmid) were expressed in HEK293T cells by calcium phosphate transfection. 16h post-transfection the medium was discarded and replaced with fresh medium. 24h later the medium was collected, centrifuged at 2500 rpm for 10 min to pellet down any cellular debris, filtered (0.22μm pore size filters) and stored at −80°C in aliquots until use. Before infection, the viruses were quantified using the SG-PERT reverse transcription assay (Vermeire et al., 2012). In brief, viral particles were lysed for 10 min at RT by adding an equal volume of 2X lysis buffer [0.25% Triton X-100, 50 mM KCl, 100 mM Tris–HCl pH 7.4, 40% glycerol and 0.8 U/μL RNase inhibitor (RiboLock, Fermentas)]. Lysates were then added to a single-step, RT-PCR assay with 3,5 nM MS2 RNA (Roche) as template, 500 nM of each primer (5′-TCCTGCTCAACTTCCTGT CGAG-3′ and 5′-CACAGGTCAAACCTCCTAGGAATG-3′), and hot-start Taq (Truestart Hotstart Taq, Fermentas), all in 20 mM Tris–Cl pH 8.3, 5 mM $(NH4)_2SO_4$, 20 mM KCl, 5 mM $MgCl_2$, 0.1 mg/ml BSA, 1/20 000 SYBR Green I (Invitrogen, #S7563), and 200 μM dNTPs. The reaction was carried out according to the following program: 42°C for 20 min for RT reaction, 95°C for 2 min for enzyme activation, followed by 40 cycles of denaturation at 95°C for 5 s, annealing at 60°C for 5 s, extension at 72°C for 15 s and acquisition at 80°C for 5 s. A standard curve was obtained using known concentrations of high-titer viral supernatants (kindly provided by Dr. Massimo Pizzato). Lentiviral particles used to express

HTT-mCherry, BDNF-mCherry, shPRMT6 and EGFP-PRMT6 in cortical neurons for the analysis of axonal trafficking were kindly produced by Aurélie Genoux.

Microfluidic devices—Microfluidic devices were prepared as previously described (Virlogeux et al., 2018). Briefly, using an epoxy resin-based V1 500 master mold (Taylor et al., 2010) we imprinted the microfluidic chamber on a mixture of silicon elastomer (PDMS) and its curing agent. Air bubbles were removed by incubation in a desiccator under vacuum for 1 h, and polymerization was performed by incubating the PDMS for 3 h at 60°C. Finalized PDMS microchambers were cut and washed with 100% ethanol followed by a quick passage through an ultrasonic bath and then washed with distilled water. Cut PDMS and glass-bottom, 0.17 μm-thick, 35 mm-diameter Petri dishes (FluoroDish, WPI) were placed into plasma cleaner under vacuum for 30 s for surface activation. After a rapid passage in an oven at 60°C, PDMS pieces were attached on Petri dishes to form an irreversible tight seal. The microfluidic devices were then coated with poly-D-lysine (0.1 mg/ml) in the upper and synaptic chambers, and with a mix of poly-D-lysine (0.1 mg/ml) + laminin (10 μg/ml) in the lower chamber overnight at 4°C. Microchambers were finally washed 3 times with growing medium (Neurobasal medium supplemented with 2% B27, 2 mM Glutamax, and 1% penicillin/streptomycin) and placed at 37°C before neuron plating.

Primary neuronal cultures in microfluidic devices—For trafficking analyses, primary cortical and striatal neurons were prepared by dissecting the cortex and the striatum from E15.5 wild-type (C57/BL6J) mouse embryos. The structures were digested with a papain/cysteine solution, followed by two incubations in trypsin inhibitor solution, and finally dissociated mechanically. Dissociated neurons were re-suspended in Neurobasal (NB) medium supplemented with B27 (2%), L-Glutamine (2 mM) and PenStrep (1%) and plated in the chamber with a final density of ~7000 cells/mm2. Cortical neurons were plated first on the upper chamber after the addition of growing medium in the synaptic chamber. Striatal neurons were subsequently added in the lower chamber. Neurons were left in the incubator for at least 3 hours, then all compartments were gently filled with growing medium. Neurons in microchambers were transduced at DIV1 and the medium was changed the day after. Acquisitions were done at DIV 12-14.

Live-cell imaging—Live-cell recordings were performed using an inverted microscope (Axio Observer, Zeiss) coupled to a spinning-disk confocal system (CSU-W1-T3, Yokogawa) connected to wide field electron-multiplying CCD camera (ProEM+1024, Princeton Instrument) and maintained at 37°C and 5% CO2. For HTT-mCherry and BDNF-mCherry trafficking, images were taken every 200 ms for 30 s (63x oil-immersion objective, 1.46 NA). Kymographs were generated using KymoToolBox plugin for ImageJ (Zala et al., 2013) to extract the following kinetics parameters (previously described in Virlogeux et al., 2018): anterograde/retrograde velocity, number of anterograde/retrograde vesicles per 100 μm, linear flow rate, directional flux. For each experiment, at least 2-3 microchambers from 3 independent neuronal cultures were used, and a minimum number of 50-60 axons were analyzed.

Immunostaining in microchambers—Neurons in microchambers were fixed with a PFA(4%)/Sucrose (4%) solution in PBS for 20 min at room temperature (RT). The fixation buffer was rinsed three times with PBS and neurons were incubated for 1h at RT with a blocking solution (1% BSA, 2% normal goat serum, 0.1% Triton X-100). The compartments of interest were then incubated with primary antibodies diluted in blocking solution overnight at 4°C and appropriate Alexa Fluor conjugated secondary antibodies (1:1000) were incubated for 1h at RT. Immunostained chambers were maintained in PBS for a maximum of one week in the dark at 4°C. The following primary antibodies were used: HTT (Merck-Millipore #MAB2166, 1:100), PRMT6 (Abcam #ab47244, 1:100), mCherry (Novus Biologicals #NBP2–25158, 1:500). Triplechannel z stack images were acquired with a × 63 oil-immersion objective (1.4 NA) using an inverted confocal microscope (LSM 710, Zeiss) coupled to an Airyscan detector to improve signal-to-noise ratio and to increase resolution. Manders' overlap coefficients (M1 and M2) were selected as colocalization indicators and calculated using the JACoP plugin v2.1.1 (Bolte and Cordeliéres, 2006) of ImageJ2/FIJI software. Input images for the JACoP plugin were the raw images kept as 3D data (x,y,z). All the images were preprocessed in the same way applying the "Despeckle" denoising filter before the colocalization analysis. Specific channel intensity thresholds required by the plugin have been optimized for the different tissues and kept constant among biological replicates.

Subcellular fractionation from whole mouse brains and primary rat neurons—Whole mouse brains were lysed in vesicle buffer (10 mM HEPES-KOH, 175 mM L-aspartic acid, 65 mM taurine, 85 mM betaine, 25 mM glycine, 6.5 mM MgCl2, 5 mM EGTA, 0.5 mM D-glucose, 1.5 mM CaCl2, 20 mM DTT, pH 7.2) containing protease inhibitors using a Dounce homogenizer. Rat neurons and STHdh$^{Q7/Q111}$ cells were lysed in IP buffer (50 mM Tris-HCl pH 7.5, 137 mM NaCl, 10 mM MgCl2,10% Glycerol, 1% Triton X-100) containing protease inhibitors. Both lysates were homogenized using a 2.5G syringe needle and subjected to sequential centrifugations at 4°C (10 min at 1200rpm, 40 min at 12000 g, 90 min at 100000 g) in order to purify a fraction enriched in nuclei (P1), a fraction containing mitochondria and large membranes such as Golgi and endoplasmic reticulum (P2), a fraction enriched in small vesicles (P3) and the corresponding cytoplasmic phases (S1, S2 and S3), as depicted in Figure 1A. Equal amounts of proteins for each fraction were loaded onto a 6% and a 10% SDS-polyacrylamide gel and examined by western blotting.

Immunogold labeling and Transmission Electron Microscopy (TEM)—For each experiment, the vesicle fraction (P3) purified from whole mouse brain was resuspended in 100-200 µl PBS and 10 µl were adsorbed to nickel formvar/carbon coated grids, fixed in 1% glutaraldehyde, washed twice with PBS, incubated with quenching solution (50 mM glycine) three times for 3 min each and blocked 10 min at RT in blocking solution (PBS +1%BSA). The first primary antibody (e.g., anti-HTT D7F7 Cell Signaling #5656, 1:30 in PBS+1%BSA) was incubated for 1h at RT, washed in PBS + 0,1% BSA and incubated with 5 nm gold anti rabbit antibody (1:50 in PBS + 1% BSA) for 30 min at RT. The grids were then washed in PBS and the protocol was repeated starting from fixation in glutaraldehyde, using the second primary antibody (e.g., anti-PRMT6 Abcam #ab47244, 1:10) and the 15 nm gold anti rabbit antibody. Finally, the grids were fixed in 1% glutaraldehyde, washed in

PBS and distilled water, and finally stained and embedded by incubation in 2% methylcellulose/5% uranyl acetate for 10 min at RT in the dark. The samples were examined using JEOL 1200 EX transmission electron microscope equipped with a digital camera (Veleta). Colocalization of HTT and PRMT6 on purified vesicles was assessed manually and compared to control conditions in which no primary antibody was used, but only the immunogold particles (5 and 15nm sizes). Three grids per conditions were analyzed, and 5 fields per grid were counted for each condition.

Quantitative real-time PCR—Total RNA was extracted with TRIzol (Invitrogen). 1 μg of RNA was reverse transcribed using iScript Reverse Transcription Supermix (Bio-Rad) following manufacturer's instructions. Gene expression was measured by quantitative real-time PCR using the iTaq Universal SYBR Green Supermix (Bio-Rad) and C1000 Touch termocycler - CFX96 Real Time System (Biorad). The level of each transcript was measured with the threshold cycle (Ct) method using GAPDH (Glyceraldehyde-3-Phosphate Dehydrogenase) mRNA as endogenous control. Primers used: PRMT6 (NM_178891.5) Fwd: AGTCCATGCTGAGCTCCGT, Rev: TCCATGCAGCTCATATCCA; PRMT2 (NM_001077638) Fwd: TCTCTGAGCCATGCACAATC, Rev: CCAGCCTTCTGGATGTCAAA; GAPDH Fwd: AACCTGCCAA GTATGATGA, Rev: GGAGTTGCTGTTGAAGTC.

Toxicity assays in striatal cells—For the measurement of cell viability in STHdh single cell clone stably expressing shRNA against PRMT2 or PRMT6, the cells were stressed for 24h with low-glucose DMEM (GIBCO #11054020) without serum and stained with LIVE/DEAD Fixable Near-IR Dead Cell Stain Kit (Thermo Fisher #L10119). The stained cells were then analyzed by using the BD (Becton Dickinson) FACSCanto flow cytometer and the FACSDiva softwareTM (version 6.1.3). For shPRMT2 stable clones, only GFP-positive cells were considered for calculating the percentage of live cells.

Toxicity assay in neurons—Primary cortical neurons were seeded on 96-well tissue culture plates at a concentration of $2.5*10^4$ cells/well. At DIV0 the immature neurons were transduced at multiplicity of infection (MOI) 3 with lentiviral particles expressing HTT 548-17Q-mCherry (wild-type or R118K) alone or HTT 548-73Q-mCherry (wild-type or R118K) together with lentiviral vectors expressing EGFP/EGFP-PRMT6 or scramble shRNA/ shRNA against PRMT6. At DIV11–12 the neurons were fixed and processed for immunocytochemistry for mCherry or mCherry/EGFPas described above. The plates were then imaged with Operetta™ High-Content Screening system (PerkinElmer). In each well, images were acquired in preselected fields (12) with LWD 20x objective over three channels with the following filter settings: λ = 360-400 nm excitation/λ = 410-480 nm emission for Hoechst, λ = 460-490 nm excitation/λ = 500-550 nm emission for anti-GFP antibody revealed by Alexa Fluor® 488, with λ = 520-550 nm excitation/λ = 590-640 nm emission for anti-mCherry antibody revealed by Alexa Fluor® 568. The images were analyzed using the Harmony software version 4.1 (PerkinElmer). Based on Hoechst staining and Alexa Fluor® 568 fluorescence intensity, nuclei and cytoplasm were respectively identified. Subpopulations of cells having red and green intensity fluorescence in the cell body above a selected threshold were selected and defined as $mCherry^+$ and GFP^+ neurons, respectively.

Finally, in each assay the total number of mCherry$^+$ or mCherry$^+$/EGFP$^+$ neurons in each condition was counted. The experiments were carried out in triplicates and repeated at least three times independently. To analyze neuronal morphology, starting from the cell body region, neurites were detected in the Alexa Fluor® 488 or Alexa Fluor® 568 channel. The building block “Find Neurites” automatically calculated for each cell a set of neurite properties such as total neurite length (sum of the length of all neurites), maximum neurite length (length of longest neurite), number of neurite segments, number of extremities (the number of ends of individual neurites).

Larval eclosion assay—Eclosion assays were performed according to the protocol in {Daigle, 2013 #243}. Briefly, ELAV-Gal4-Geneswitch driver lines (FlyBase FBtp0015149) were crossed to UAS-PRMT6, UAS-HTT16Q (FlyBase FBst0033810), UAS-HTT128Q (FlyBase FBti0139921), UAS-PRMT6;UAS-HTT16Q, UAS-PRMT6;UAS-HTT128Q, or *w1118* (CTRL) linesin5 biological replicates on standard cornmeal medium. Crosses were then transferred to fresh vials containing medium with 10 μM RU-486 (Cayman Chemical #10006317) every 24 hours until exhausted. Progeny were cultured at 25°C, and the number of pupated larvae in each vial was recorded. Eclosion rates were then compared by binomial tests between crosses, with successes defined as eclosion events, and failures defined as pupae failing to emerge after 2 weeks of monitoring. Eclosed adults were discarded immediately to prevent contamination.

Larval preparation, immunohistochemistry and quantification—For analysis of axonal blockages and the neuromuscular junction (NMJ), *w1118* (CTRL) or HTT 128Q flies were crossed with ElavGS as well as ElavGS;PRMT6 combo lines and raised on standard cornmeal at 28°C in light/dark controlled incubators. First instar larvae were collected and transferred to RU-486 (Mifepristone, Cayman Chemical, #10006317) (Anderson et al., 2018). Wondering third instar larvae were dissected, fixed, and immunostained (Gunawardena and Goldstein, 2001). Briefly, larvae were dissected in PBS and fixed in 4% paraformaldehyde in PBS for 20 min at room temperature, washed 3 times with 0.1% PBST (0.1% Triton X-100 in PBS), and then blocked with 5% normal goat serum (NGS) (Abcam; AB7681) in 0.1% PBST. Larvae were then probed with primary antibody mouse anti-DCSP3 (DSHB, IG12, 1:100) overnight at 4°C. Larvae were then washed three times in 0.1 % PBST and incubated in secondary antibodies (anti-mouse Alexa Flour 647, Invitrogen, # 28181, 1:100) and Cy3-conjugated anti-HRP (Jackson ImmunoResearch, Cat#: 123-165-021, 1:200) for 2 hours, washed three times in 0.1% PBST, and mounted using DAPi Fluoroshield (SIGMA, #F6182). Images were collected using NIKON A1 eclipse T_i confocal. For the analysis, NMJ from muscle 4 on segment A2-A3 were imaged from 4-5 larvae, and the synaptic boutons were quantified using ImageJ software (NIH).

Quantitative analysis on blockages was carried out by collecting confocal images of larval neurons from the region directly below or posterior to the larval brain, where several segmental nerves are visible or come into focus through the optical series. The number of axonal blocks per larvae was measured with ImageJ software. Briefly, we thresholded background noise in control animals’ segmental nerves before quantifying our experimental condition. CSP blocks are easily distinguished from signals such as neuromuscular junction/

synaptic boutons (see the bright signal in Figure 6A) based on the Horseradish peroxidase (HRP) staining. At least three optical images were taken for each larva (5 larvae per condition, for a total of at least 15 images) and the quantification was performed on these images. This quantification and imaging protocol have been well established and are routinely used in our labs (Anderson et al., 2020; Gunawardena and Goldstein, 2001; Xu et al., 2016).

QUANTIFICATION AND STATISTICAL ANALYSIS

For each experiment, the quantification method has been described in the corresponding STAR Methods section. Statistical analysis was performed using GraphPad Prism8 (GraphPad Software, San Diego, CA). For all experiments, the normality of the data was assessed using a D'Agostino-Pearson test. The data were considered normally distributed with $\alpha = 0.05$. Statistical significance for comparison of two groups was determined either by the parametric Student's t test or the non-parametric Mann-Whitney test. For multiple comparisons, statistical significance was determined by one-way ANOVA followed by parametric or non-parametric post hoc tests according to the distribution of the data. All data are presented as mean ± SEM. The number of experimental replicates and the specific tests used are reported in the figure legend for each experiment. Statistically significant results were defined as follows: *$p < 0.05$; **$p < 0.01$; ***$p < 0.001$; $p < 0.0001$****. The p value is reported in the figures and legends for each experiment.

Supplementary Material

Refer to Web version on PubMed Central for supplementary material.

ACKNOWLEDGMENTS

We thank V. Brandt for critical reading of the manuscript; members of the Transcriptional Neurobiology lab and the labs of M. Pennuto, S. Humbert, and F. Saudou for comments; the Model Organism Facility and The High-throughput Screening Facility (in particular Michael Pancher) at Department CIBIO; the GIN imaging facility (PIC-GIN) for help with image acquisitions; A. Genoux for virus production regarding the experiments performed in microchambers; and T. Léger and C. Garcia from the Plateforme Protéomique Structurale et Fonctionnelle from the Institut Jacques Monod, CNRS Université Paris-Di-derot. We would like to thank Dr. Elena Cattaneo for providing the pCAG-Htt1955-15Q construct and advice on the protocol for HTT immunoprecipitation. This work has been performed in the framework of Bando Progetti Strategici di Ateneo – University of Trento (M.P. and M.B.). This work was supported by grants from Telethon-Italy and Autonomous Province of Trento (TCP12013 to M.P.); Association Française contre les Myopathies (AFM-22221 to M.P. and M.B.); PRIN-MUR (2017F2A2C5 to M.P.); National Institutes of Health (1R21NS111768-01 to M.P. and U.B.P.); PROGRAM RARE DISEASES CNCCS-Scarl-Pomezia (M.P.); FONDAZIONE AIRC-Italy (24423 to M.P.); Alzheimer Trento Onlus with the legato Baldrachi (M.B.); the Agence Nationale de la Recherche (ANR-15-JPWG-0003-05 JPND CIRCPROT and ANR-18-CE16-0009-01 AXYON to F.S.); Fédération pour la Recherche sur le Cerveau (F.S.); the AGEMED program from Inserm (F.S.); NeuroCoG in the framework of the "Investissements d'avenir" program (ANR-15-IDEX-02 to F.S.); and the Spanish Ministry of Science, Innovation and Universities (RTI2018-096322-B-I00 MCIU/AEI/FEDER-UE to J.J.L.). The F.S. laboratory is member of the Grenoble Center of Excellence in Neurodegeneration (GREEN). A.M. was recipient of a fellowship funded by the University of Trento. A.M. was supported by a Boehringer Ingelheim Fonds travel grant and an EMBO STF (STF-8140). C.S. was supported by a postdoctoral fellowship from FRM and by EMBO LTF (ALTF 693-2015). The graphical abstract was created with BioRender.com.

REFERENCES

Albrecht LV, Ploper D, Tejeda-Muñoz N, and De Robertis EM (2018). Arginine methylation is required for canonical Wnt signaling and endolysosomal trafficking. Proc. Natl. Acad. Sci. USA 115, E5317–E5325. [PubMed: 29773710]

Anderson EN, Gochenaur L, Singh A, Grant R, Patel K, Watkins S, Wu JY, and Pandey UB (2018). Traumatic injury induces stress granule formation and enhances motor dysfunctions in ALS/FTD models. Hum. Mol. Genet 27, 1366–1381. [PubMed: 29432563]

Anderson EN, Hirpa D, Zheng KH, Banerjee R, and Gunawardena S (2020). The non-amyloidal component region of α-synuclein is important for α-synuclein transport within axons. Front. Cell. Neurosci 13, 540. [PubMed: 32038170]

Arbez N, Ratovitski T, Roby E, Chighladze E, Stewart JC, Ren M, Wang X, Lavery DJ, and Ross CA (2017). Post-translational modifications clustering within proteolytic domains decrease mutant huntingtin toxicity. J. Biol. Chem 232, 19238–19249.

Baric I, Fumic K, Glenn B, Cuk M, Schulze A, Finkelstein JD, James SJ, Mejaski-Bosnjak V, Pazanin L, Pogribny IP, et al. (2004). S-adenosylhomocysteine hydrolase deficiency in a human: a genetic disorder of methionine metabolism. Proc. Natl. Acad. Sci. USA 101, 4234–4239. [PubMed: 15024124]

Barnat M, Capizzi M, Aparicio E, Boluda S, Wennagel D, Kacher R, Kassem R, Lenoir S, Agasse F, Braz BY, et al. (2020). Huntington's disease alters human neurodevelopment. Science 369, 787–793. [PubMed: 32675289]

Basso M, and Pennuto M. (2015). Serine phosphorylation and arginine methylation at the crossroads to neurodegeneration. Exp. Neurol 271, 77–83. [PubMed: 25979114]

Basso M, Berlin J, Xia L, Sleiman SF, Ko B, Haskew-Layton R, Kim E, Antonyak MA, Cerione RA, lismaa SE, et al. (2012). Transglutaminase inhibition protects against oxidative stress-induced neuronal death downstream of pathological ERK activation. J. Neurosci 32, 6561–6569. [PubMed: 22573678]

Ben M'Barek K, Pla P, Orvoen S, Benstaali C, Godin JD, Gardier AM, Saudou F, David DJ, and Humbert S. (2013). Huntingtin mediates anxiety/depression-related behaviors and hippocampal neurogenesis. J. Neurosci 33, 8608–8620. [PubMed: 23678106]

Blanc RS, and Richard S. (2017). Arginine methylation: the coming of age. Mol. Cell 65, 8–24. [PubMed: 28061334]

Bolte S, and Cordeliéres FP (2006). A guided tour into subcellular colocalization analysis in light microscopy. J. Microsc 224, 213–232. [PubMed: 17210054]

Chaibva M, Jawahery S, Pilkington AW 4th, Arndt JR, Sarver O, Valentine S, Matysiak S, and Legleiter J. (2016). Acetylation within the first 17 residues of huntingtin exon 1 alters aggregation and lipid binding. Biophys. J 111, 349–362. [PubMed: 27463137]

Chang B, Chen Y, Zhao Y, and Bruick RK (2007). JMJD6 is a histone arginine demethylase. Science 318, 444–447. [PubMed: 17947579]

Chang K-H, Chen Y-C, Wu Y-R, Lee W-F, and Chen C-M (2012). Downregulation of genes involved in metabolism and oxidative stress in the peripheral leukocytes of Huntington's disease patients. PLoS ONE 7, e46492. [PubMed: 23029535]

Chiki A, DeGuire SM, Ruggeri FS, Sanfelice D, Ansaloni A, Wang ZM, Cendrowska U, Burai R, Vieweg S, Pastore A, et al. (2017). Mutant exon1 huntingtin aggregation is regulated by T3 phosphorylation-induced structural changes and crosstalk between T3 phosphorylation and acetylation at K6. Angew. Chem. Int. Ed. Engl 56, 5202–5207. [PubMed: 28334491]

Chitiprolu M, Jagow C, Tremblay V, Bondy-Chorney E, Paris G, Savard A, Palidwor G, Barry FA, Zinman L, Keith J, et al. (2018). A complex of C9ORF72 and p62 uses arginine methylation to eliminate stress granules by autophagy. Nat. Commun 9, 2794. [PubMed: 30022074]

Colin E, Zala D, Liot G, Rangone H, Borrell-Pagés M, Li XJ, Saudou F, and Humbert S. (2008). Huntingtin phosphorylation acts as a molecular switch for anterograde/retrograde transport in neurons. EMBO J. 27, 2124–2134. [PubMed: 18615096]

Dompierre JP, Godin JD, Charrin BC, Cordelières FP, King SJ, Humbert S, and Saudou F. (2007). Histone deacetylase 6 inhibition compensates for the transport deficit in Huntington's disease by increasing tubulin acetylation. J. Neurosci 27, 3571–3583. [PubMed: 17392473]

Friesen WJ, Massenet S, Paushkin S, Wyce A, and Dreyfuss G. (2001). SMN, the product of the spinal muscular atrophy gene, binds preferentially to dimethylarginine-containing protein targets. Mol. Cell 7, 1111–1117. [PubMed: 11389857]

Fu MM, and Holzbaur ELF (2014). MAPK8IP1/JIP1 regulates the trafficking of autophagosomes in neurons. Autophagy 10, 2079–2081. [PubMed: 25483967]

Fuhrmann J, and Thompson PR (2016). Protein arginine methylation and citrullination in epigenetic regulation. ACS Chem. Biol 11, 654–668. [PubMed: 26686581]

Gauthier LR, Charrin BC, Borrell-Pagès M, Dompierre JP, Rangone H, Cordelières FP, De Mey J, MacDonald ME, Lessmann V, Humbert S, and Saudou F. (2004). Huntingtin controls neurotrophic support and survival of neurons by enhancing BDNF vesicular transport along microtubules. Cell 118, 127–138. [PubMed: 15242649]

Gindhart JG Jr., Desai CJ, Beushausen S, Zinn K, and Goldstein LSB (1998). Kinesin light chains are essential for axonal transport in Drosophila. J. Cell Biol 141, 443–454. [PubMed: 9548722]

Guccione E, and Richard S. (2019). The regulation, functions and clinical relevance of arginine methylation. Nat. Rev. Mol. Cell Biol 20, 642–657. [PubMed: 31350521]

Gunawardena S, and Goldstein LSB (2001). Disruption of axonal transport and neuronal viability by amyloid precursor protein mutations in Drosophila. Neuron 32,389–401. [PubMed: 11709151]

Gunawardena S, Her L-S, Brusch RG, Laymon RA, Niesman IR, Gordesky-Gold B, Sintasath L, Bonini NM, and Goldstein LSB (2003). Disruption of axonal transport and neuronal viability by amyloid precursor protein mutations in Drosophila. Neuron 40, 25–40. [PubMed: 14527431]

Guo A, Gu H, Zhou J, Mulhern D, Wang Y, Lee KA, Yang V, Aguiar M, Kornhauser J, Jia X, et al. (2014). Immunoaffinity enrichment and mass spectrometry analysis of protein methylation. Mol. Cell. Proteomics 13, 372–387. [PubMed: 24129315]

Hahn P, Wegener I, Burrells A, Böse J, Wolf A, Erck C, Butler D, Schofield CJ, Böttger A, and Lengeling A. (2010). Analysis of Jmjd6 cellular localization and testing for its involvement in histone demethylation. PLoS ONE 5, e13769. [PubMed: 21060799]

Hinckelmann MV, Zala D, and Saudou F. (2013). Releasing the brake: restoring fast axonal transport in neurodegenerative disorders. Trends Cell Biol. 23, 634–643. [PubMed: 24091156]

Hinckelmann MV, Virlogeux A, Niehage C, Poujol C, Choquet D, Hoflack B, Zala D, and Saudou F. (2016). Self-propelling vesicles define glycolysis as the minimal energy machinery for neuronal transport. Nat. Commun 7, 13233. [PubMed: 27775035]

Hofweber M, Hutten S, Bourgeois B, Spreitzer E, Niedner-Boblenz A, Schifferer M, Ruepp MD, Simons M, Niessing D, Madl T, and Dormann D (2018). Phase separation of FUS is suppressed by its nuclear import receptor and arginine methylation. Cell 173, 706–719.e13. [PubMed: 29677514]

Humbert S, Bryson EA, Cordelières FP, Connors NC, Datta SR, Fink-beiner S, Greenberg ME, and Saudou F (2002). The IGF-1/Akt pathway is neuroprotective in Huntington's disease and involves Huntingtin phosphorylation by Akt. Dev. Cell 2, 831–837. [PubMed: 12062094]

Jeong H, Then F, Melia TJ Jr., Mazzulli JR, Cui L, Savas JN, Voisine C, Paganetti P, Tanese N, Hart AC, et al. (2009). Acetylation targets mutant huntingtin to autophagosomes for degradation. Cell 137, 60–72. [PubMed: 19345187]

Klinman E, Tokito M, and Holzbaur ELF (2017). CDK5-dependent activation of dynein in the axon initial segment regulates polarized cargo transport in neurons. Traffic 18, 808–824. [PubMed: 28941293]

Locasale JW (2013). Serine, glycine and one-carbon units: cancer metabolism in full circle. Nat. Rev. Cancer 13, 572–583. [PubMed: 23822983]

Maday S, Twelvetrees AE, Moughamian AJ, and Holzbaur ELF (2014). Axonal transport: cargo-specific mechanisms of motility and regulation. Neuron 84, 292–309. [PubMed: 25374356]

Magiera MM, Bodakuntla S, Žiak J, Lacomme S, Marques Sousa P, Leboucher S, Hausrat TJ, Bosc C, Andrieux A, Kneussel M, et al. (2018). Excessive tubulin polyglutamylation causes neurodegeneration and perturbs neuronal transport. EMBO J. 37, e100440. [PubMed: 30420556]

Menalled LB, Sison JD, Wu Y, Olivieri M, Li X-J, Li H, Zeitlin S, and Chesselet M-F (2002). Early motor dysfunction and striosomal distribution of huntingtin microaggregates in Huntington's disease knock-in mice. J. Neurosci 22, 8266–8276. [PubMed: 12223581]

Millecamps S, and Julien J-P (2013).Axonal transport deficits and neurodegenerative diseases. Nat. Rev. Neurosci 14, 161–176. [PubMed: 23361386]

Morfini GA, Burns M, Binder LI, Kanaan NM, LaPointe N, Bosco DA, Brown RH Jr., Brown H, Tiwari A, Hayward L, et al. (2009). Axonal transport defects in neurodegenerative diseases. J. Neurosci 29, 12776–12786. [PubMed: 19828789]

Morfini G, Schmidt N, Weissmann C, Pigino G, and Kins S (2016). Conventional kinesin: Biochemical heterogeneity and functional implications in health and disease. Brain Res. Bull 126, 347–353. [PubMed: 27339812]

Osterwalder T, Yoon KS, White BH, and Keshishian H. (2001). A conditional tissue-specific transgene expression system using inducible GAL4. Proc. Natl. Acad. Sci. USA 98, 12596–12601. [PubMed: 11675495]

Paul BD, Sbodio JI, Xu R, Vandiver MS, Cha JY, Snowman AM, and Snyder SH (2014). Cystathionine α-lyase deficiency mediates neurodegeneration in Huntington's disease. Nature 509, 96–100. [PubMed: 24670645]

Phalke S, Mzoughi S, Bezzi M, Jennifer N, Mok WC, Low DHP, Thike AA, Kuznetsov VA, Tan PH, Voorhoeve PM, and Guccione E. (2012). p53-Independent regulation of p21Waf1/Cip1 expression and senescence by PRMT6. Nucleic Acids Res. 40, 9534–9542. [PubMed: 22987071]

Qamar S, Wang G, Randle SJ, Ruggeri FS, Varela JA, Lin JQ, Phillips EC, Miyashita A, Williams D, Ströhl F, et al. (2018). FUS phase separation is modulated by a molecular chaperone and methylation of arginine cation-π interactions. Cell 173, 720–734.e15. [PubMed: 29677515]

Ratovitski T, Chighladze E, Arbez N, Boronina T, Herbrich S, Cole RN, and Ross CA (2012). Huntingtin protein interactions altered by polyglutamine expansion as determined by quantitative proteomic analysis. Cell Cycle 11, 2006–2021. [PubMed: 22580459]

Ratovitski T, Arbez N, Stewart JC, Chighladze E, and Ross CA (2015). PRMT5-mediated symmetric arginine dimethylation is attenuated by mutant huntingtin and is impaired in Huntington's disease (HD). Cell Cycle 14, 1716–1729. [PubMed: 25927346]

Ratovitski T, O'Meally RN, Jiang M, Chaerkady R, Chighladze E, Stewart JC, Wang X, Arbez N, Roby E, Alexandris A, et al. (2017). Post-translational modifications (PTMs), identified on endogenous huntingtin, cluster within proteolytic domains between HEAT repeats. J. Proteome Res 16, 2692–2708. [PubMed: 28653853]

Saudou F, and Humbert S. (2016). The Biology of Huntingtin. Neuron 89, 910–926. [PubMed: 26938440]

Scaramuzzino C, Monaghan J, Milioto C, Lanson NA Jr., Maltare A, Aggarwal T, Casci I, Fackelmayer FO, Pennuto M, and Pandey UB (2013). Protein arginine methyltransferase 1 and 8 interact with FUS to modify its sub-cellular distribution and toxicity in vitro and in vivo. PLoS ONE 8, e61576. [PubMed: 23620769]

Scaramuzzino C, Casci I, Parodi S, Lievens PMJ, Polanco MJ, Milioto C, Chivet M, Monaghan J, Mishra A, Badders N, et al. (2015). Protein arginine methyltransferase 6 enhances polyglutamine-expanded androgen receptor function and toxicity in spinal and bulbar muscular atrophy. Neuron 85, 88–100. [PubMed: 25569348]

Schneider CA, Rasband WS, and Eliceiri KW (2012). NIH Image to ImageJ: 25 years of image analysis. Nat. Methods 9, 671–675. [PubMed: 22930834]

Schulte J, and Littleton JT (2011). The biological function of the Huntingtin protein and its relevance to Huntington's Disease pathology. Curr. Trends Neurol 5, 65–78. [PubMed: 22180703]

Steffan JS, Agrawal N, Pallos J, Rockabrand E, Trotman LC, Slepko N, Illes K, Lukacsovich T, Zhu Y-Z, Cattaneo E, et al. (2004). SUMO modification of Huntingtin and Huntington's disease pathology. Science 304, 100–104. [PubMed: 15064418]

Subramaniam S, Sixt KM, Barrow R, and Snyder SH (2009). Rhes, a striatal specific protein, mediates mutant-huntingtin cytotoxicity. Science 324, 1327–1330. [PubMed: 19498170]

Tapia O, Bengoechea R, Palanca A, Arteaga R, Val-Bernal JF, Tizzano EF, Berciano MT, and Lafarga M (2012). Reorganization of Cajal bodies and nucleolar targeting of coilin in motor neurons of type I spinal muscular atrophy. Histochem. Cell Biol 137, 657–667. [PubMed: 22302308]

Tartari M, Gissi C, Lo Sardo V, Zuccato C, Picardi E, Pesole G, and Cattaneo E. (2008). Phylogenetic comparison of huntingtin homologues reveals the appearance of a primitive polyQ in sea urchin. Mol. Biol. Evol 25,330–338. [PubMed: 18048403]

Taylor AM, Dieterich DC, Ito HT, Kim SA, and Schuman EM (2010). Microfluidic local perfusion chambers for the visualization and manipulation of synapses. Neuron 66, 57–68. [PubMed: 20399729]

Thompson PR, and Fast W. (2006). Histone citrullination by protein arginine deiminase: is arginine methylation a green light or a roadblock? ACS Chem. Biol 1,433–441. [PubMed: 17168521]

Trettel F, Rigamonti D, Hilditch-Maguire P, Wheeler VC, Sharp AH, Persichetti F, Cattaneo E, and MacDonald ME (2000). Dominant phenotypes produced by the HD mutation in STHdh(Q111) striatal cells. Hum. Mol. Genet 9,2799–2809. [PubMed: 11092756]

Tripathy D, Vignoli B, Ramesh N, Polanco MJ, Coutelier M, Stephen CD, Canossa M, Monin M-L, Aeschlimann P, Turberville S, et al. (2017). Mutations in TGM6 induce the unfolded protein response in SCA35. Hum. Mol. Genet 26, 3749–3762. [PubMed: 28934387]

Trushina E, Dyer RB, Badger JD 2nd, Ure D, Eide L, Tran DD, Vrieze BT, Legendre-Guillemin V, McPherson PS, Mandavilli BS, et al. (2004). Mutant huntingtin impairs axonal trafficking in mammalian neurons in vivo and in vitro. Mol. Cell. Biol 24, 8195–8209. [PubMed: 15340079]

Vance C, Rogelj B, Hortobágyi T, De Vos KJ, Nishimura AL, Sreedharan J, Hu X, Smith B, Ruddy D, Wright P, et al. (2009). Mutations in FUS, an RNA processing protein, cause familial amyotrophic lateral sclerosis type 6. Science 323, 1208–1211. [PubMed: 19251628]

Vermeire J, Naessens E, Vanderstraeten H, Landi A, Iannucci V, Van Nuffel A, Taghon T, Pizzato M, and Verhasselt B. (2012). Quantification of reverse transcriptase activity by real-time PCR as a fast and accurate method for titration of HIV, lenti- and retroviral vectors. PLoS ONE 7, e50859. [PubMed: 23227216]

Virlogeux A, Moutaux E, Christaller W, Genoux A, Bruyère J, Fino E, Charlot B, Cazorla M, and Saudou F (2018). Reconstituting corticostriatal network on-a-chip reveals the contribution of the presynaptic compartment to Huntington's Disease. Cell Rep. 22, 110–122. [PubMed: 29298414]

Wang Y, Wysocka J, Sayegh J, Lee YH, Perlin JR, Leonelli L, Sonbuchner LS, McDonald CH, Cook RG, Dou Y, et al. (2004). Human PAD4 regulates histone arginine methylation levels via demethylimination. Science 306, 279–283. [PubMed: 15345777]

Wang JZ, Xia YY, Grundke-Iqbal I, and Iqbal K. (2013). Abnormal hyperphosphorylation of tau: sites, regulation, and molecular mechanism of neurofibrillary degeneration. J. Alzheimers Dis 33 (Suppl 1), S123–S139. [PubMed: 22710920]

Wang F, He L, Huangyang P, Liang J, Si W, Yan R, Han X, Liu S, Gui B, Li W, et al. (2014). JMJD6 promotes colon carcinogenesis through negative regulation of p53 by hydroxylation. PLoS Biol. 12, e1001819. [PubMed: 24667498]

Webby CJ, Wolf A, Gromak N, Dreger M, Kramer H, Kessler B, Nielsen ML, Schmitz C, Butler DS, Yates JR 3rd., et al. (2009). Jmjd6 catalyses lysyl-hydroxylation of U2AF65, a protein associated with RNA splicing. Science 325, 90–93. [PubMed: 19574390]

Wesche J, Kühn S, Kessler BM, Salton M, and Wolf A. (2017). Protein arginine methylation: a prominent modification and its demethylation. Cell. Mol. Life Sci 74, 3305–3315. [PubMed: 28364192]

Wong YC, and Holzbaur ELF (2014). The regulation of autophagosome dynamics by huntingtin and HAP1 is disrupted by expression of mutant huntingtin, leading to defective cargo degradation. J. Neurosci 34, 1293–1305. [PubMed: 24453320]

Xu W, Weissmiller AM, White JA 2nd, Fang F, Wang X, Wu Y, Pearn ML, Zhao X, Sawa M, Chen S, et al. (2016). Amyloid precursor protein-mediated endocytic pathway disruption induces axonal dysfunction and neurodegeneration. J. Clin. Invest 126, 1815–1833. [PubMed: 27064279]

Yanai A, Huang K, Kang R, Singaraja RR, Arstikaitis P, Gan L, Orban PC, Mullard A, Cowan CM, Raymond LA, et al. (2006). Palmitoylation of huntingtin by HIP14 is essential for its trafficking and function. Nat. Neurosci 9, 824–831. [PubMed: 16699508]

Zala D, Colin E, Rangone H, Liot G, Humbert S, and Saudou F. (2008). Phosphorylation of mutant huntingtin at S421 restores anterograde and retrograde transport in neurons. Hum. Mol. Genet 17, 3837–3846. [PubMed: 18772195]

Zala D, Hinckelmann MV, Yu H, Lyra da Cunha MM, Liot G, Cordelières FP, Marco S, and Saudou F (2013). Vesicular glycolysis provides on-board energy for fast axonal transport. Cell 152, 479–491. [PubMed: 23374344]

Zhao X, Feng Z, Ling KKY, Mollin A, Sheedy J, Yeh S, Petruska J, Narasimhan J, Dakka A, Welch EM, et al. (2016). Pharmacokinetics, pharmacodynamics, and efficacy of a small-molecule SMN2 splicing modifier in mouse models of spinal muscular atrophy. Hum. Mol. Genet 25, 1885–1899. [PubMed: 26931466]

Highlights

- Arginine methylation regulates huntingtin (HTT)-mediated trafficking
- The arginine methyltransferase PRMT6 methylates vesicle-associated HTT
- Loss of arginine methylation hampers HTT recruitment to vesicles and neuronal viability
- PRMT6 expression rescues effects of mutant HTT on trafficking *in vitro* and *in vivo*

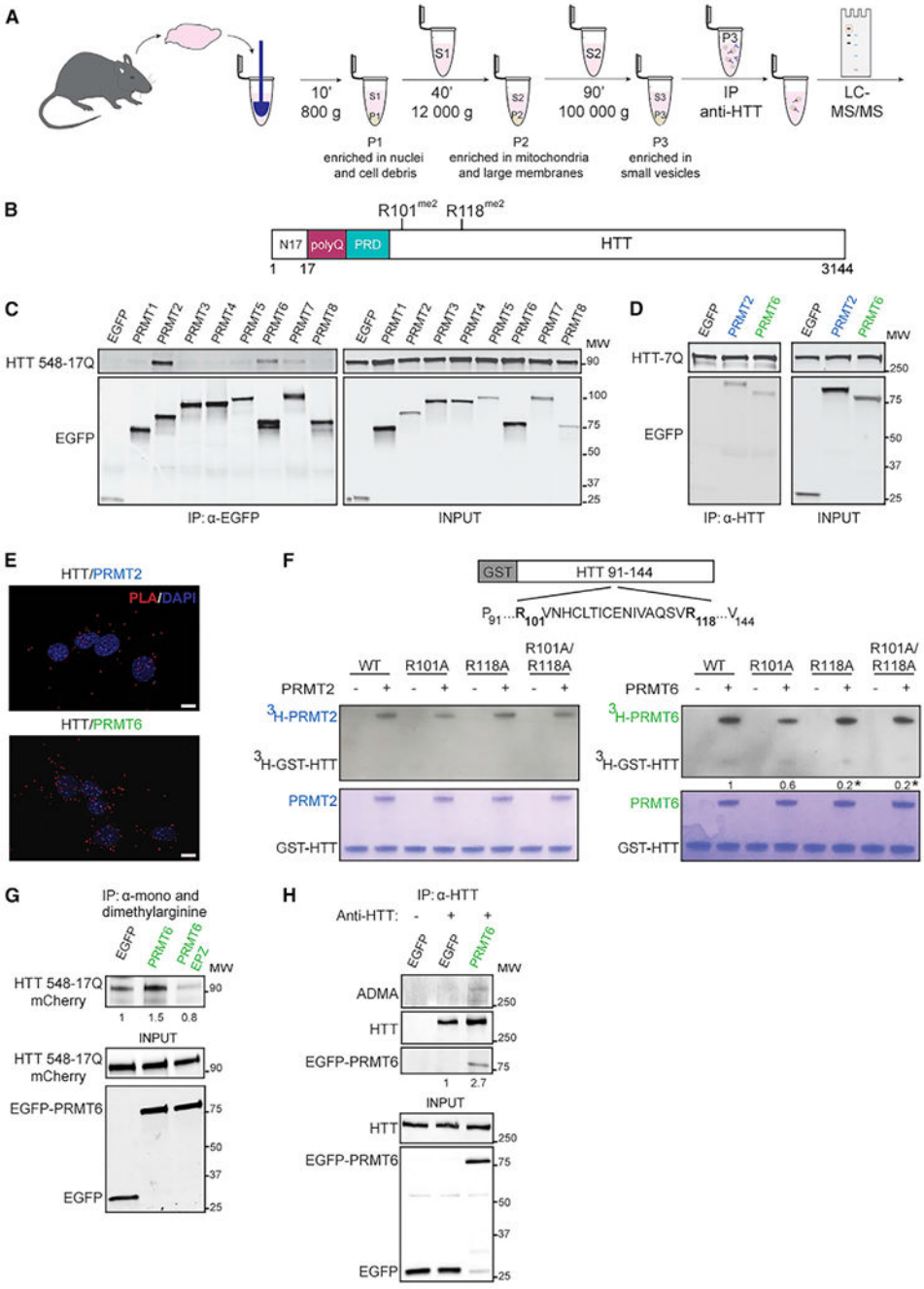

Figure 1. Vesicle-associated HTT is methylated at R118 by PRMT6

(A and B) Schematic of vesicle-associated HTT purification from mouse brain for liquid chromatography-tandem mass spectrometry (LC-MS/MS) analysis and identification of methylated arginine residues (R101 and R118). N17, N-terminal 17 amino acids; PRD, proline-rich domain; polyQ, polyglutamine tract.

(C) Immunoprecipitation (IP) assay in HEK293T cells overexpressing HTT 548-17Q together with either soluble EGFP or EGFP-tagged PRMT1–PRMT8. Shown is one experiment out of four.

(D) IP assay in STHdh$^{Q7/Q7}$ cells overexpressing EGFP-PRMT2 or EGFP-PRMT6. Shown is one experiment representative of four.
(E) Proximity ligation assay (PLA) in STHdh$^{Q7/Q7}$ cells. Nuclei were revealed with DAPI. Shown are representative images from three independent experiments. Bar, 10 μm.
(F) *In vitro* methylation assay performed by incubating wild-type or mutant GST-HTT fusion proteins and recombinant PRMT2 (left panel) or PRMT6 (right panel) in the presence of [^{3}H]-SAM. Top: fluorography. Bottom: Coomassie Brilliant blue staining. Shown is one experiment representative of two. Student's t test, *$p < 0.05$. Quantification (average) of [^{3}H]-HTT/HTT ratio is shown at the bottom of the fluorography panel.
(G) IP assay with an anti-mono- and di-methylarginine antibody in mouse cortical neurons overexpressing HTT 548-17Q-mCherry together with soluble EGFP or EGFP-PRMT6 treated or not with EPZ (10 μM). Shown is a representative image from at least two independent experiments. Quantification (average) of HTT IP/HTT input ratio is shown at the bottom of the IP panel.
(H) IP assay in primary rat cortical neurons transduced with a lentiviral vector expressing EGFP or EGFP-PRMT6. Shown is one experiment representative of two. Quantification (average) of asymmetric dimethylarginine/HTT signal ratio is shown at the bottom of the IP panel.

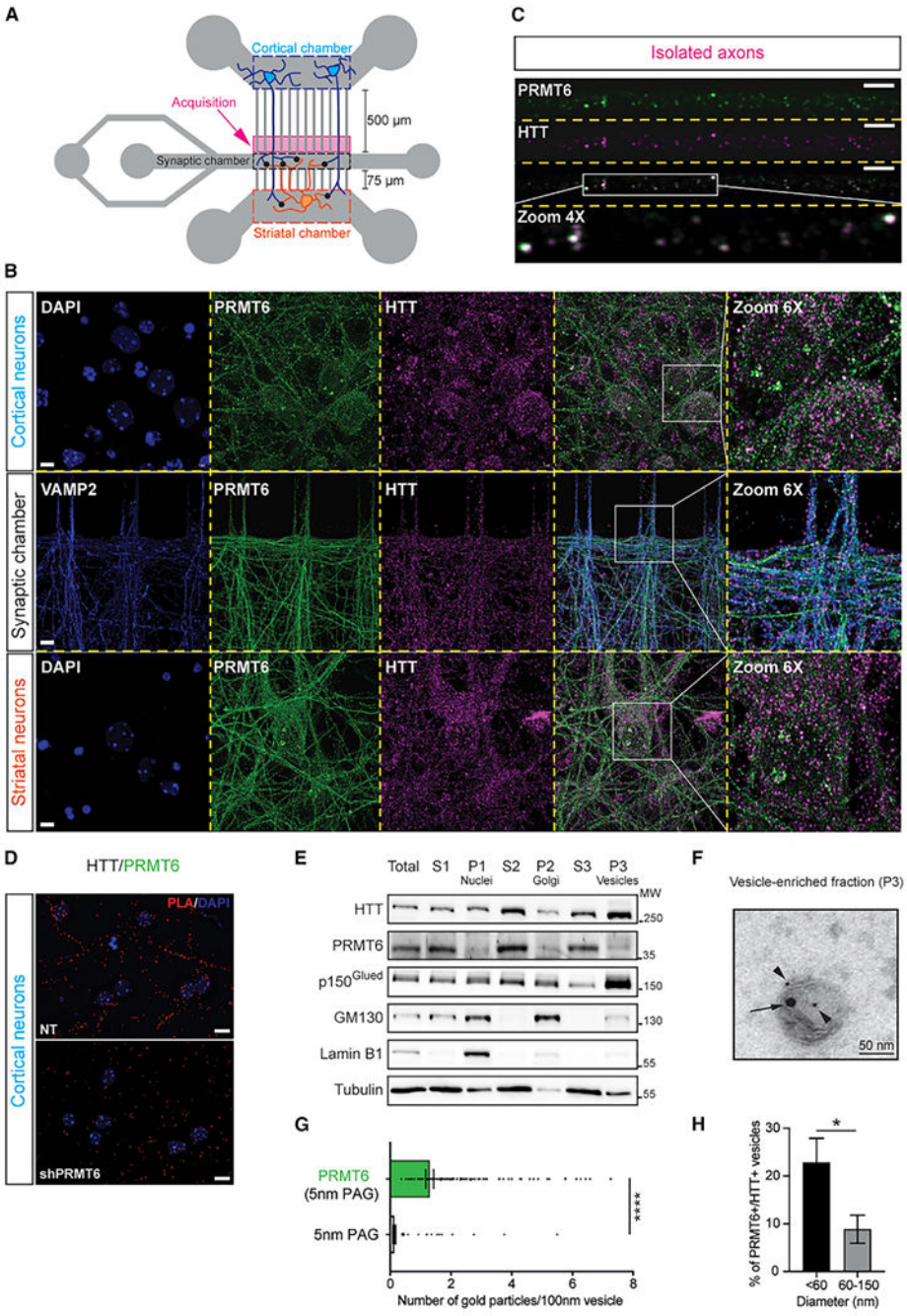

Figure 2. PRMT6 colocalizes with HTT in axons and is present in brain-derived vesicles

(A) Schematic depicting the microfluidic chamber reconstituting the corticostriatal network.

(B and C) Immunofluorescence analysis of PRMT6 and HTT in DIV14 mouse primary neurons plated in microfluidic chambers as in (A). Bars, 5 µm (B) and 2 µm (C). Shown are representative images from three independent experiments.

(D) PLA in cortical neurons. Nuclei were visualized with DAPI. Shown are representative images from three independent experiments. Bar, 10 µm.

(E) Subcellular fractionation of mouse brain extracts. Purity of fractions was verified by immunoblotting for the presence of laminB1 (nuclear marker), GM130 (Golgi marker), and $p150^{Glued}$ (enriched in the P3 fraction). S1, S2, and S3 represent the corresponding cytosolic fractions. Shown is one experiment representative of three.

(F) Immunogold transmission electron microscopy (TEM) analysis of the P3 fraction from (E). PRMT6 is indicated with an arrowhead (5 nm gold nanoparticles); HTT is indicated with an arrow (15 nm gold nanoparticles). Shown is one representative image from three independent experiments. Bar, 50 nm.

(G) Quantification of immunogold-labeled vesicles isolated from mouse brain from (F). PRMT6, 5nm gold nanoparticles with anti-PRMT6 primary antibody; 5 nm PAG, negative control without anti-PRMT6 primary antibody. Student's t test, ****$p < 0.0001$; $n_{CTRL} = 188$ and $n_{PRMT6} = 174$.

(H) Quantification of the percentage of PRMT6 and HTT-positive vesicles. PRMT6, 5 nm gold particles; HTT, 15 nm particles. Student's t test, *$p < 0.05$.

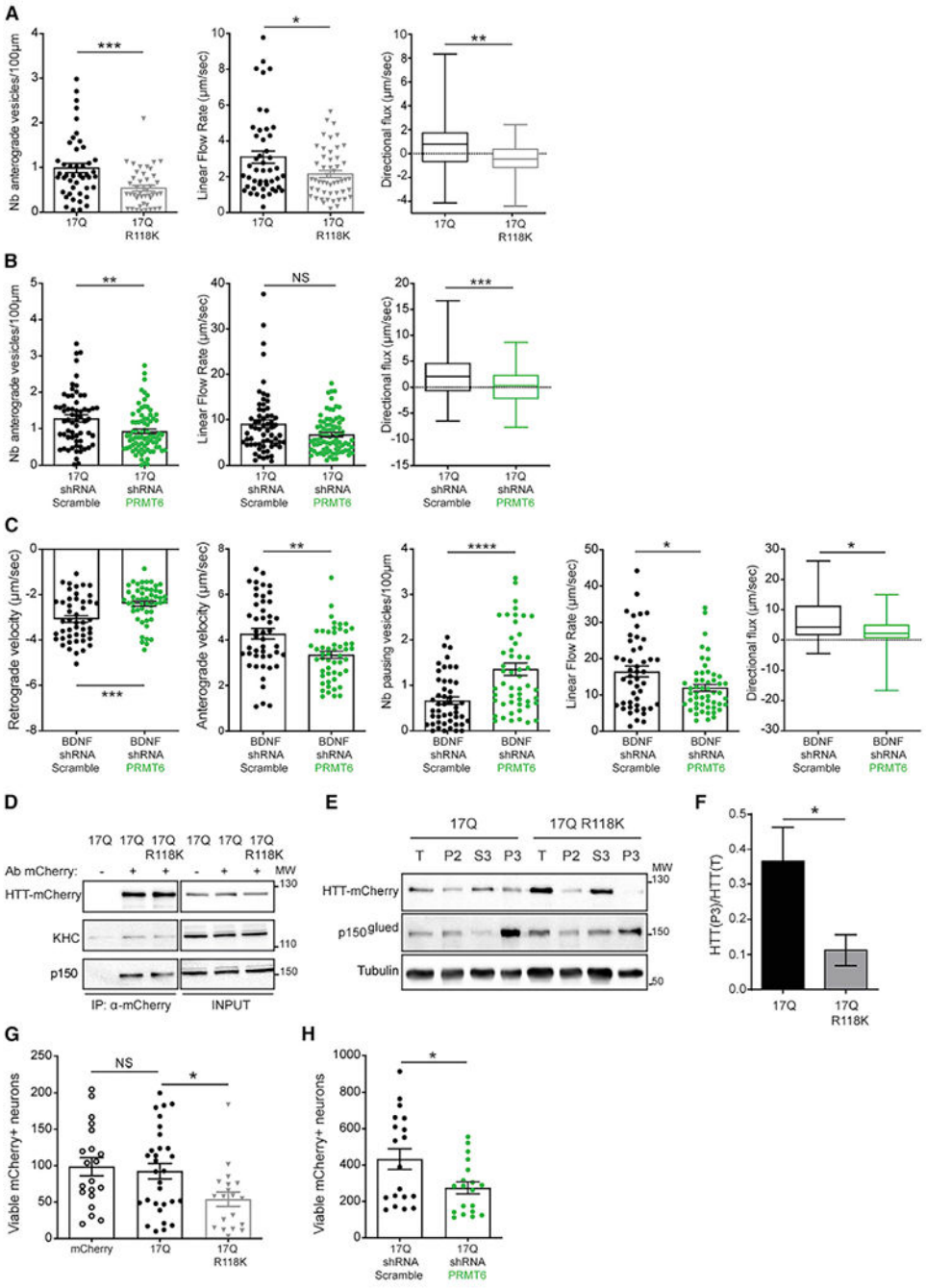

Figure 3. Methylation of HTT at R118 regulates its participation in axonal trafficking

(A) Analysis of the trafficking kinetics in DIV14 cortical neurons transduced with lentiviral vectors expressing either wild-type HTT 548-17Q or HTT 548-17Q R118K fused to mCherry. Two-tailed non-parametric Mann-Whitney test, *p < 0.05, **p < 0.01, and ***p < 0.001.

(B) Analysis of trafficking kinetics in DIV14 cortical neurons transduced with lentiviral vectors expressing wild-type HTT 548-17Q fused to mCherry together with scrambled or

PRMT6 shRNA. Two-tailed non-parametric Mann-Whitney test, **p < 0.01 and ***p < 0.001; NS, not significant.

(C) Analysis of the trafficking kinetics in DIV14 cortical neurons transduced with lentiviral vectors expressing BDNF-mCherry together with scrambled or PRMT6 shRNA. Two-tailed non-parametric Mann-Whitney test, *p < 0.05, **p < 0.01, ***p < 0.001, and ****p < 0.0001.

(D) Immunoprecipitation assay in primary rat neurons transduced with mCherry-tagged HTT 548-17Q or HTT 548-17Q R118K.

(E) Immunoblotting analysis of subcellular fractionation of primary rat cortical neurons transduced as in (A). Shown is one experiment representative of three.

(F) Quantification of HTT 548-mCherry signal in the P3 fraction over total fraction from (C). Graph shows mean ± SEM; n = 3. Student's t test, *p < 0.05

(G) Analysis of cell viability in DIV11 mouse primary cortical neurons expressing either mCherry or HTT 548-17Q-mCherry or HTT 548-17Q R118K-mCherry. The total number of viable $mCherry^+$ neurons in each condition was calculated using the Operetta High-Content Imaging system. Graph shows mean ± SEM; n = 3. One-way ANOVA, Tukey's post hoc test, *p < 0.05; NS, not significant.

(H) Analysis of cell viability in DIV11 mouse primary cortical neurons transduced with lentiviral vectors expressing HTT 548-17Q fused to mCherry together with scrambled or PRMT6 shRNA. The total number of viable $mCherry^+$ neurons in each condition was calculated using the Operetta High-Content Imaging system. Graph shows mean ± SEM; n = 4. One-way ANOVA, Tukey's post hoc test, *p < 0.05.

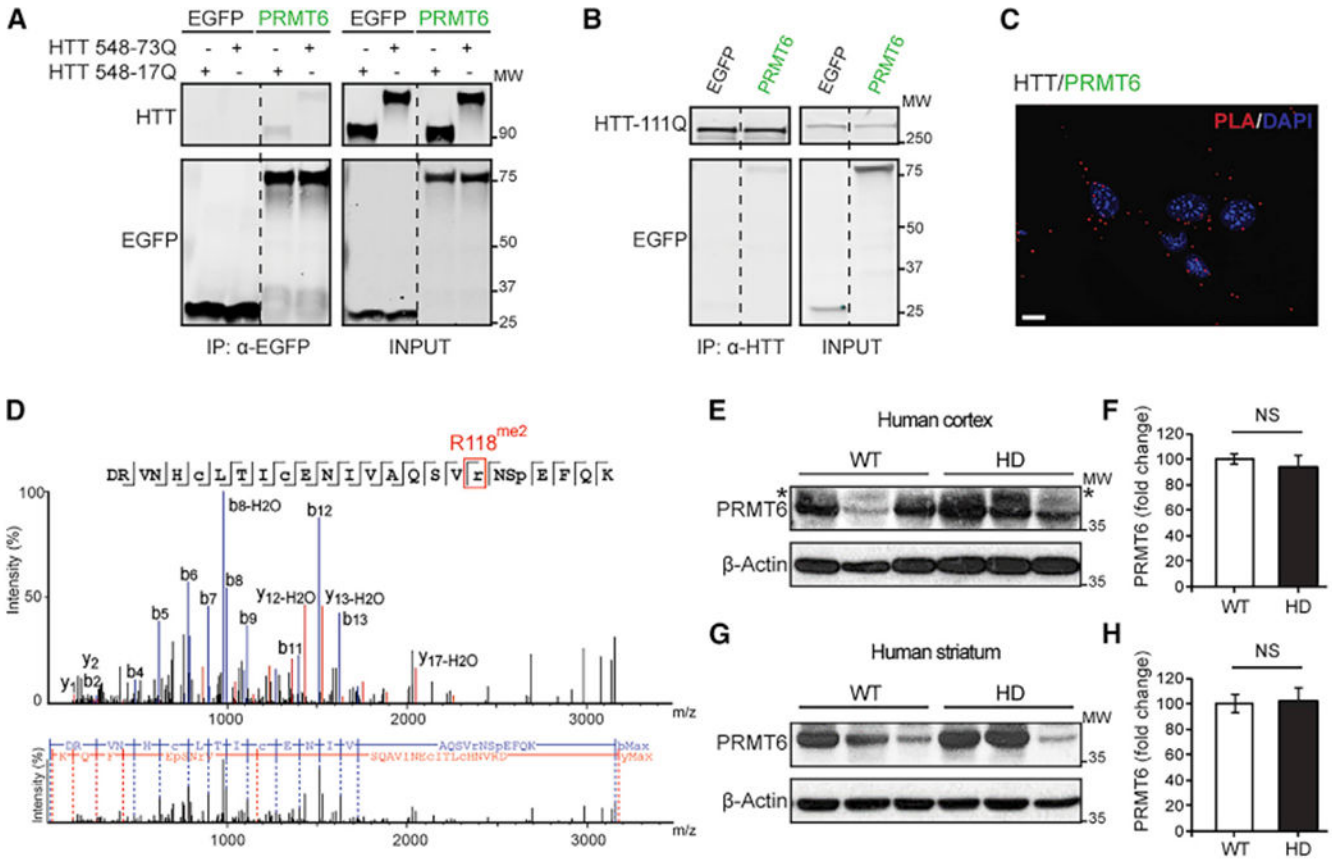

Figure 4. Interaction with PRMT6 and R118 methylation are preserved in mHTT

(A) CoIP assay in HEK293T cells overexpressing wild-type (HTT 548-17Q) or mutant N-terminal HTT (HTT 548-73Q) together with soluble EGFP or EGFP-tagged PRMT6. Shown is one experiment out of four. Dashed line indicates that lanes were run on the same gel but were noncontiguous. The original blot is shown in Figure S7A.

(B) CoIP assay in STHdh$^{Q111/Q111}$ cells overexpressing EGFP or EGFP-PRMT6. Shown is one experiment out of four. Dashed line indicates that lanes were run on the same gel but were noncontiguous. The original blot is shown in Figure S7B.

(C) PLA in STHdh$^{Q111/Q111}$ cells. Nuclei were revealed with DAPI. Shown are representative images from three independent experiments. Bar, 10 μm.

(D) Electrospray ionization (ESI)-MS/MS analysis of human full-length mHTT (HTT-82Q) purified from transfected HEK293 cells.

(E and G) Immunoblotting analysis of PRMT6 expression in the cortex (E) and striatum (G) of HD patients or healthy individuals.

(F and H) Quantification of (E) and (G), respectively. Graph shows mean ± SEM; n = 3. Student's t test. NS, not significant.

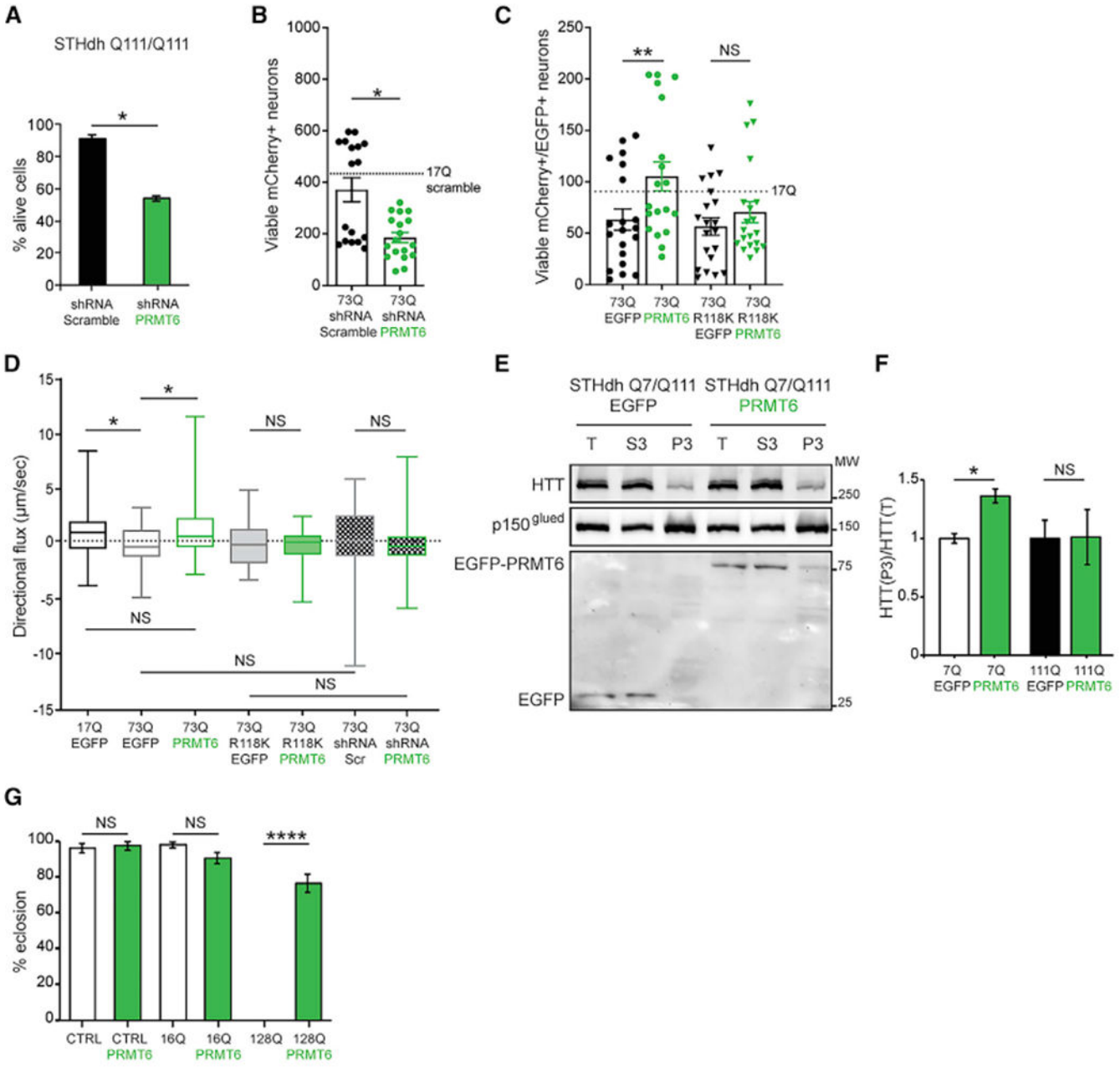

Figure 5. PRMT6 modifies mHTT-induced toxicity

(A) Cell viability assay in STHdh$^{Q111/Q111}$ single-cell clones stably expressing a scramble shRNA or an shRNA against PRMT6. Graph shows mean ± SEM; n = 3. Student's t test, *p < 0.05. Single independent experiments are shown in Figure S8.

(B) Analysis of cell viability in DIV11 mouse primary cortical neurons transduced with lentiviral vectors expressing HTT 548-73Q fused to mCherry together with scrambled or PRMT6 shRNA. The total number of viable mCherry^{+} neurons in each condition was calculated using the Operetta High-Content Imaging system. Graph shows mean ± SEM; n = 4. One-way ANOVA, Tukey's post hoc test, *p < 0.05.

(C) Analysis of cell viability in mouse primary cortical neurons expressing mCherry-tagged HTT 548-73Q or HTT 548-73Q R118K together with EGFP or EGFP-PRMT6. The total number of viable $mCherry^{+}/EGFP^{+}$ neurons in each condition was calculated using the Operetta High-Content Imaging system. Graph shows mean ± SEM; n = 4. Two-way ANOVA, Tukey's post hoc test, **p < 0.01; NS, not significant.
(D) Analysis of the trafficking kinetics in DIV12–DIV14 neurons transduced with lentiviral vectors expressing mCherry-tagged HTT 548-17Q, HTT 548-73Q, or HTT 548-73Q R118K together with EGFP, EGFP-PRMT6, scrambled shRNA, and PRMT6 shRNA. Graph shows mean ± SEM; n = 3. Kruskal-Wallis test, Dunn's post hoc, *p < 0.05; NS, not significant.
(E) Immunoblotting analysis of subcellular fractionation of $STHdh^{Q7/Q111}$ transduced with EGFP or EGFP-PRMT6 lentivirus. Shown is one experiment representative of three.
(F) Quantification of HTT and mHTT signals in the P3 fraction over total fraction from (E). Graph shows mean ± SEM; n = 3. Student's t test, *p < 0.05.
(G) Eclosion assays in control flies or flies expressing full-length HTT 16Q or HTT 128Q. The number of pupae analyzed is between 70 and 100 for each experimental group. Graph shows mean ± SEM, n = 5. Two-way ANOVA, Tukey's post hoc test, ****p < 0.0001; NS, not significant.

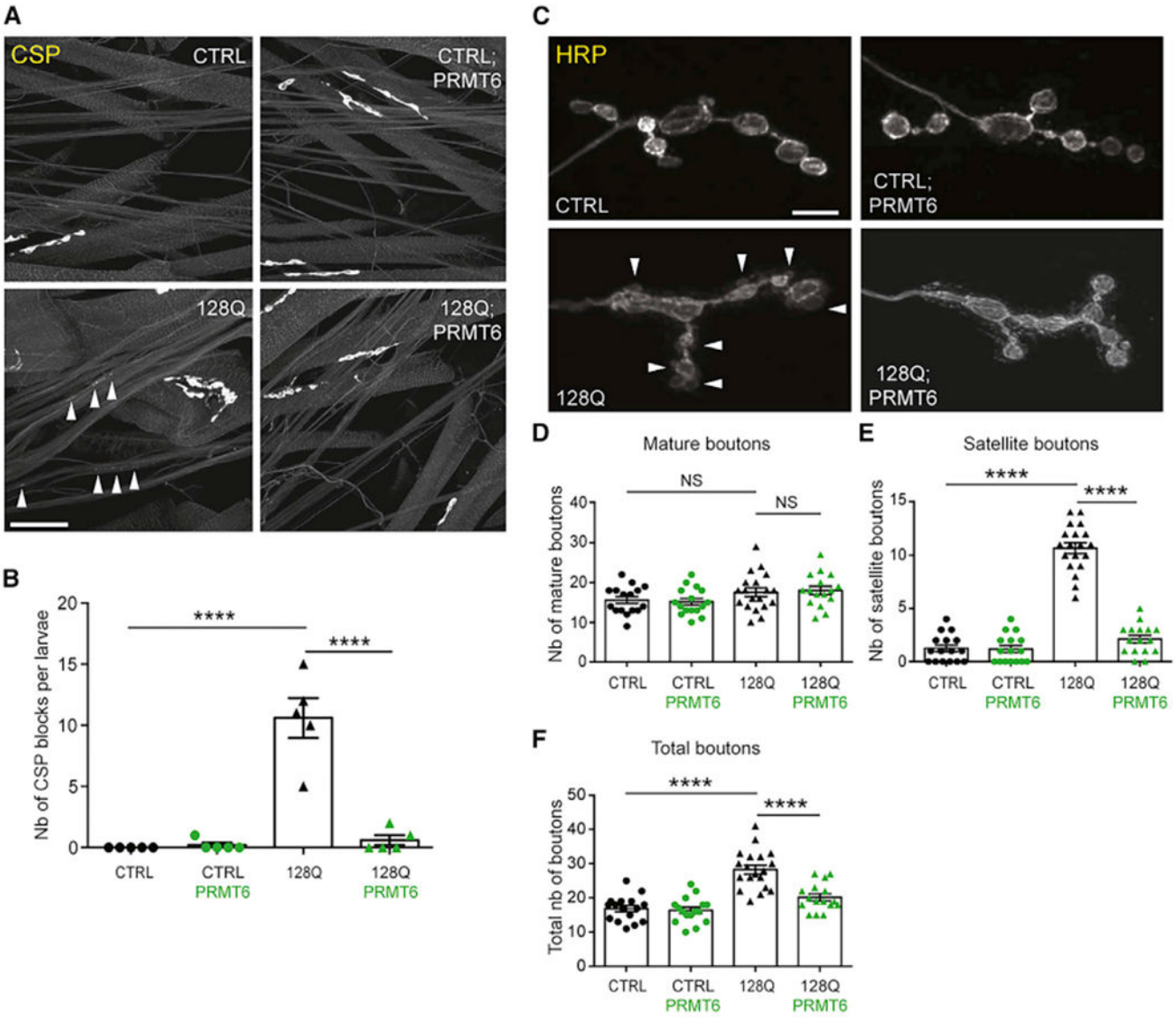

Figure 6. PRMT6 expression rescues HTT-mediated axonal and neuromuscular junction (NMJ) defects in *Drosophila*

(A) Representative larval segmental nerves from ELAV-GeneSwitch (ElavGS); *w1118* (CTRL), PRMT6 (PRMT6; *w1118*), HTT 128Q (128Q), or PRMT6; HTT 128Q (PRMT6; 128Q) larvae (CSP, cysteine string protein [arrowhead]). Bar, 15 μM.

(B) Quantification of CSP blocks in (A) (****$p < 0.0001$, $n = 5$).

(C) Immunofluorescence images of neuromuscular junctions at muscle 4 segment A2-A3 stained with the presynaptic marker horseradish peroxidase (HRP; arrowhead). Bar, 10 μM.

(D–F) Quantification of the average number of mature boutons (D) and satellite boutons (E) and the total number of boutons (F) ($n = 16–19$). Graphs in (B) and (D)–(F) represent mean ± SEM. Statistical comparison in (B) and (D)–(F) were determined using one-way ANOVA with Tukey's multiple comparisons test (*$p < 0.05$ and ****$p < 0.0001$; NS, not significant).

KEY RESOURCES TABLE

REAGENT or RESOURCE	SOURCE	IDENTIFIER
Antibodies		
Rabbit monoclonal anti-huntingtin (D7F7)	Cell Signaling Technology	Cat#5656; RRID: AB_10827977
Mouse monoclonal anti-huntingtin (clone 1HU-4C8)	Merck Millipore	Cat#MAB2166; RRID: AB_11213141
Mouse monoclonal anti-polyQ (clone MW1)	Developmental Studies Hybridoma Bank, DSHB (University of Iowa)	Cat#MW1; RRID: AB_528290
Mouse monoclonal anti-GFP (clones 7.1 and 13.1)	Roche	Cat# 11814460001; RRID: AB_390913
Chicken polyclonal anti-GFP	Thermo Fisher Scientific	Cat#A10262; RRID: AB_2534023
Mouse monoclonal anti-GFP	Merck Millipore	Cat#MAB2510; RRID: AB_94623
Rabbit polyclonal anti-mCherry	Institute Curie	Cat#A-P-R#13
Rabbit polyclonal anti-mCherry	Thermo Fisher Scientific	Cat#PA5-34974; RRID: AB_2552323
Chicken polyclonal anti-mCherry	Novus Biologicals	Cat#NBP2-25158; RRID: AB_2636881
Rabbit polyclonal anti-PRMT6	Bethyl Laboratories	Cat#A300-929A; RRID: AB_2237733
Rabbit polyclonal anti-PRMT6	Proteintech	Cat#15395-1-AP; RRID: AB_2237723
Rabbit polyclonal anti-PRMT6	Abcam	Cat#ab47244; RRID: AB_2284473
Rabbit polyclonal anti-PRMT2	Abcam	Cat#ab66763; RRID: AB_1142323
Mouse monoclonal anti-tubulin	Sigma Aldrich	Cat#T7816; RRID: AB_261770
Mouse monoclonal anti-mono- and dimethylarginine [76E]	Abcam	Cat#ab412; RRID: AB_304292
Rabbit polyclonal anti-asymmetric dimethylarginine	Merck Millipore	Cat#07-414; RRID: AB_310596
Mouse monoclonal anti-p150 [Glued]	BD Transduction Laboratories	Cat#610474; RRID: AB_397846
Mouse monoclonal anti-KHC [clone SUK4]	Covance Antibody Products	Cat#MMS-188P; RRID: AB_2028782
Rabbit monoclonal anti-GM130 [EP892Y]	Abcam	Cat#ab52649; RRID: AB_880266
Mouse monoclonal anti-GM130	BD Transduction Laboratories	Cat#610822; RRID: AB_398141
Rabbit polyclonal anti-Lamin B1	Abcam	Cat#ab16048; RRID: AB_443298
Rabbit monoclonal anti-Lamin B1	Abcam	Cat# ab133741; RRID: AB_2616597
Rabbit polyclonal anti-Calnexin	Enzo Life Sciences	Cat#ADI-SPA-860F; RRID: AB_11178981
Rabbit polyclonal anti-Calnexin	Sigma Aldrich	Cat#C4731; RRID: AB_476845
Rabbit polyclonal anti-Histone H3	Genetex	Cat#GTX122148; RRID: AB_10633308
Rabbit polyclonal anti-Histone H3R8me2a	Active Motif	Cat#39651; RRID: AB_2793290
Mouse monoclonal anti-MAP2 [HM-2]	Abcam	Cat#ab11267; RRID: AB_297885

REAGENT or RESOURCE	SOURCE	IDENTIFIER
Chicken polyclonal anti-MAP2	Merck Millipore	Cat#AB15452; RRID: AB_805385
IRDye® 680RD Goat anti-Mouse IgG Secondary Antibody	LI-COR	Cat#926-68070; RRID AB_10956588
IRDye® 800CW Goat anti-Rabbit IgG Secondary Antibody	LI-COR	Cat#926-32211: RRID AB_621843
IRDye® 800CW Donkey anti-Chicken Secondary Antibody	LI-COR	Cat#926-32218: RRID AB_1850023
Mouse anti-rabbit IgG-HRP	Santa Cruz	Cat#sc-2357; RRID: AB_628497
m-IgGκ BP-HRP	Santa Cruz	Cat#sc-516102; RRID: AB_2687626
Goat anti-Rabbit IgG (H+L)-Alexa Fluor 488	Thermo Fisher Scientific	Cat#A-11008; RRID: AB_143165
Goat anti-Mouse IgG (H+L)-Alexa Fluor 647	Thermo Fisher Scientific	Cat#A-21235; RRID: AB_2535804
Goat anti-Chicken IgY (H+L)-Alexa Fluor 555	Thermo Fisher Scientific	Cat# A-21437; RRID: AB_2535858
Goat anti-Rabbit IgG (H+L)-Alexa Fluor 568	Thermo Fisher Scientific	Cat#A-11011; RRID: AB_143157
Goat anti-Mouse IgG (H+L)-Alexa Fluor 488	Thermo Fisher Scientific	Cat#A-11001; RRID: AB_2534069
Bacterial and virus strains		
E.coli Rosetta (DE3)	Dr. Laura Tosatto	N/A
Biological samples		
Brain specimens (frontal cortex and striatum) of control and HD subjects, see Table S3	Institute of Neuropathology (HUB-ICO-IDIBELL) Brain Bank (Hospitalet de Llobregat, Spain)/Neurological Tissue Bank of the IDIBAPS Biobank (Barcelona, Spain); Banco de Tejidos Fundación Cien (BT-CIEN, Madrid, Spain)	N/A
Chemicals, peptides, and recombinant proteins		
Human recombinant PRMT2	Active Motif	Cat#31392
Human recombinant PRMT6	Active Motif	Cat#31394
Human recombinant Histone H3.1	NEB	Cat#M2503S
Protein A Sepharose beads	Sigma Aldrich	Cat#P9424
Protein A/G Plus Agarose beads	Santa Cruz	Cat#sc-2003
cOmplete, EDTA-free Protease Inhibitor Cocktail	Roche	Cat#11873580001
DNase I recombinant	Roche	Cat#4536282001
Isopropyl β-D-1-thiogalactopyranoside (IPTG)	AppliChem	Cat#A4773,0025
Pierce® Glutathione Agarose	Thermo Scientific	Cat#16100
L-Glutathione reduced	Sigma Aldrich	Cat #G4251
Recombinant GST-HTT 91-144	This paper	N/A
Recombinant GST-HTT 91-144 R101A	This paper	N/A
Recombinant GST-HTT 91-144 R118A	This paper	N/A

REAGENT or RESOURCE	SOURCE	IDENTIFIER
Recombinant GST-HTT 91-144 R101A/R118A	This paper	N/A
Adenosine-2,3-dialdehyde (Adox)	Sigma Aldrich	Cat#A7154
S-(5′-Adenosyl)-L-methionine (SAM)	Sigma Aldrich	Cat#A7007
EPZ020411	MedChemExpress	Cat#HY-12970A
RU-486 (Mifepristone)	Cayman Chemica	Cat#10006317
Poly-D-lysine	Sigma Aldrich	Cat#P7280
Hoechst	Sigma Aldrich	Cat#B2261
Polyethylenimine (PEI)	Sigma Aldrich	Cat#408727
Eagles' Balanced Salt Solution (EBSS)	Sigma Aldrich	Cat#E7510
Papain	Sigma Aldrich	Cat#P4762
L-Cystine	Sigma Aldrich	Cat#C7602
DNase I	Sigma Aldrich	Cat#D5025
Trypsin inhibitor	Sigma Aldrich	Cat#T9253
Ara-C	Sigma Aldrich	Cat#C1768
Bovine serum albumin (BSA)	Sigma Aldrich	Cat#A7030
Critical commercial assays		
Duolink PLA kit	Sigma-Aldrich	Cat#DUO92101
LIVE/DEAD Fixable Near-IR Dead Cell Stain Kit	Thermo Fisher Scientific	Cat#L10119
Experimental models: cell lines		
HEK293T Cells	Dr. Alberto Inga	N/A
STHdh Cells	Dr. Marcy E. MacDonald; Trettel et al., 2000	N/A
Experimental models: organisms/strains		
C57BL/6J	Charles River	N/A
$Hdh^{CAG140/+}$	From Dr. Scott Zeitlin lab; Menalled et al., 2002	N/A
ELAV-Gal4-GeneSwitch	Bloomington stock center	Cat#43642
w1118 (CTRL)	Bloomington stock center	Cat#3605
UAS-HTT16Q	Bloomington stock center	Cat#33810
UAS-HTT128Q	Bloomington stock center	Cat#33808
UAS-PRMT6	This paper	N/A
Oligonucleotides		
PRMT6 primers for qPCR: Fwd AGTCCATGCTGAGCTCCGT, Rev TCCATGCAGCTCATATCCA	This paper	N/A
PRMT2 primers for qPCR: Fwd TCTCTGAGCCATGCACAATC, Rev CCAGCCTTCTGGATGTCAAA	This paper	N/A
GAPDH primers for qPCR: Fwd AACCTGCCAAGTATGATGA, Rev GGAGTTGCTGTTGAAGTC	This paper	N/A
Recombinant DNA		
Htt N586 22Q	Arbez et al., 2017	N/A
Htt N586 82Q	Arbez et al., 2017	N/A
pCAG HTT N548-17Q	Dr. Elena Cattaneo	N/A

REAGENT or RESOURCE	SOURCE	IDENTIFIER
pCAG HTT N548-73Q	This paper	N/A
pCAG HTT N548-17Q R118K	This paper	N/A
pCAG HTT N548-73Q R118K	This paper	N/A
Lenti HTT N548-17Q	This paper	N/A
Lenti HTT N548-73Q	This paper	N/A
Lenti HTT N548-17Q R118K	This paper	N/A
Lenti HTT N548-73Q R118K	This paper	N/A
pGEX-6P-3	Dr. Paolo Struffi	N/A
pGEX-6P-3 HTT 91-144	This paper	N/A
pGEX-6P-3 HTT 91-144 R101A	This paper	N/A
pGEX-6P-3 HTT 91-144 R118A	This paper	N/A
pGEX-6P-3 HTT 91-144 R101A/R118A	This paper	N/A
EGFP-PRMTs	Dr. F.O. Fackelmayer	N/A
EGFP-PRMT6 V86K,D88A	Scaramuzzino et al., 2013	N/A
Lenti EGFP-PRMT6	This paper	N/A
PRMT2 shRNA (pGFP-C-shLenti vector)	Origene	Cat#TL500997
PRMT6 shRNA (pLKO.1-puro vector)	Dr. Ernesto Guccione, Phalke et al., 2012	N/A
psPAX2	Dr. Massimo Pizzato	Addgene #12260
pMD2.G	Dr. Massimo Pizzato	Addgene #12259
LV. SIN.VAMP2.mCherry	Dr. Tim Ryan	N/A
LV.CMV.BDNF-mCherry	Hinckelmann et al., 2016	N/A
Software and algorithms		
FACSDiva software™ (version 6.1.3)	Becton Dickinson	https://www.bdbiosciences.com/en-us/instruments/research-instruments/research-software/flow-cytometry-acquisition/facsdiva-software
(Fiji is just) ImageJ 1.52	Schneider et al., 2012	https://imagej.nih.gov/ij
Adobe Illustrator	Adobe	https://www.adobe.com/products/illustrator.html
GraphPad Prism 8	GraphPad Software	https://www.graphpad.com/scientific-software/prism/
MaxQuant software package version 1.2.2.5	MPI for Biochemistry, Germany	https://www.maxquant.org/
Other		
Lipofectamine 2000 Transfection reagent	Thermo Fisher Scientific	Cat#11668019
ProLong Diamond Antifade Mountant	Thermo Fisher Scientific	Cat#P36961
Amaxa Nucleofector™	Lonza	Cat#AAB-1001